Mathematical Modeling of a Network of Neurons Regarding Glucose Transport Deficiency Induced Epileptic Seizures

by

ARIEL N. LESLIE

Presented to the Faculty of the Graduate School of
The University of Texas at Arlington in Partial Fulfillment
of the Requirements
for the Degree of

DOCTOR OF PHILOSOPHY

THE UNIVERSITY OF TEXAS AT ARLINGTON

December 2019

To God and my family, you heard me even in my silence.

Thank you.

ACKNOWLEDGEMENTS

First and foremost, I would like to thank God for His guidance and faithfulness. I cannot go on without thanking the University of Texas at Arlington (UTA) Department of Mathematics Graduate Assistance for Areas of National Need via the US Department of Education for financially supporting my PhD education and research. I must also thank the National Science Foundation (NSF) for funding my studies through the Louis Stokes Alliance for Minority Participation Bridge to the Doctorate Fellowship (Grant No. HRD-1026806). Extensive courses, projects, summer research and dissertaation research all cumlminates to this very paper, a PhD level dissertation. I would also like to thank Texas Southern University professors: Dr. Willie Taylor, Dr. Roderick Holmes, Dr. A. Serpil Saydam, Dr. Joan Evans, and Dr. Robert Nehs for their moral and mathematical support. I could never forget University of Houston professor, Dr. Mark Tomforde for his many lessons of grit and determination.

Secondly, I would like to thank my advisor Dr. Juanzhong Su for all of his guidance and expertise throughout my research and writing process. I would not be able to navigate the PhD and thesis process without his support. His mathematical knowledge has helped me in my graduate studies, academic career, in addition to graduate level research. I'd also wish to thank my advising committee, Dr. Li Wang, Dr. Hristo Kojouharov, and Dr. Ren-Cang Li for their help and support during my academic career at UTA. In addition to the academic guidance through hard times. To all of my mentors: Dr. Minerva Cordero, Dr. Kayunta Johnson-Winters,

Dr. Tuncay Aktosun and the late Dr. Alisa Johnson for giving me advice or simply lending a helping hand when I needed it most. Your assistance will never be forgotten. You all have shaped my mathematical abilities in preparation for a great future.

Next, I want to express my unending gratitude to Lona, Libby, Laura, Zach, Michael, Jasmine, and Angel for their time, advice, and assistance throughout the program. I would not have been able to survive and thrive in graduate school without my close friends Mayowa, Kimoi, Imelda, Iris, Talon, Dwight, John, Crystal, Sita, Dillon, Anthony, Gul, and Emel. Thank you so much for your friendship. Your smiles and positive affirmations are just what I needed.

Finally, to my family and close friends, thank you for praying for me. Thank you to my parents for believing in me, no matter the situation. Thank you to my sweet husband Charles who consistently pushed me to strive for better every day. Thank you to my parents (Barron and Stephanie) and bonus parents (Mrs. Gabe and Donna), sisters (Jordan, Milani, and Jameelah), grandmothers, grandfather, aunts and uncles, and extended family for believing in me. I love and appreciate all of you.

November 13, 2019

ABSTRACT

Mathematical Modeling of a Network of Neurons Regarding Glucose Transport Deficiency Induced Epileptic Seizures

Ariel N. Leslie, Ph.D.

The University of Texas at Arlington, 2019

Supervising Professor: Dr. Jianzhong Su

Epilepsy is a complex phenomena of a system of neurons simultaneously firing that are highly intensive and synchronized. Seizures are a common and well known physical feature for all types of epileptic disorders [8]. Epilepsy is known to be traced back to spatial and temporal patterns working in sequence. The rhythms, patterns, and oscillatory dynamics explain the mechanistic nature of neurons especially in absence seizures [37]. An electroencephalogram device (EEG) monitors the electrical activity within the brain using small electrodes, which measures voltage fluctuations on the scalp. Previous models such as Wilson-Cowan (1972) [34], introduced a model showing the dynamics of a network of neurons consisting of excitatory and inhibitory neurons. Taylor et. al (2014) then adapted the Wilson-Cowan model to epileptic seizures using a thalamo-cortical based theory. Fan et. al (2018) projects that thalamic reticulus nuclei control spike wave discharges specifically in absence seizures.G1D Transport Deficiency Epilepsy can be identified by the high number of seizures during the infant stage which is usually rapid, irregular eye movement, and small brain size. We want to identify brain activity specific to G1D by using

EEG data. Additionally, we want to study the EEG patterns to identify the plausible mechanism that causes G1D epileptic behavior. The goal is to find out how an entirely connected brain network shows the neuronal functionality as a unit regarding G1D. Our coupled thalamo-cortical model goes beyond a connection in a logical unidirectional pattern shown by Fan (2018) or in a bidirectional small world pattern. Our model is a network based on paired correlation of EEG signals more analogous to realistic seizure activity. Using our model, we are able to study stability analysis for equilibrium and periodic behavior, parameter values which cause synchronized activity or more stable activity and identify a synchronization index, and sensitivity analysis regarding parameters that directly affect Spike Wave Discharges and other spiking behavior. We will show how our 32-unit network model reflects G1D seizure dynamics and discuss the limitations of the model.

TABLE OF CONTENTS

CHAPTER 1

INTRODUCTION

In this work, we aim to produce a mathematical model of Glucose Transport Deficiency induced Epilepsy, specifically, the model that depicts the intrinsic brain activity seen from EEG before and after a seizure, thoroughly understand the unique neuronal activity produced by this neurological disease and also study the biological inferences gained from a mathematical analysis of a network of neurons with regards to Glucose Transport Deficiency Epilepsy. The importance of this research study lies in the wide range of severity of symptoms and in fact the patient population itself. According to the National Organization for Rare Diseases, symptoms vary drastically from patient to patient. Many times, individuals with mild symptoms either go undiagnosed or misdiagnosed. Other times, these symptoms lead to very serious and disabling complications.

Signs include one of five different types of seizures: most commonly known tonic or clonic, myoclonic, atypical absence, atonic and unclassified.

In our case, we will study motifs of absence seizures. Absence seizures are also known as petit mal seizures. This particular type of seizure starts on both sides of the brain simultaneously. The duration of time for these seizures is very brief, typically only a few seconds from onset to the end. A major reason for misdiagnosis is, this seizure causes lapse in awareness, staring, daydreaming, and or glazed over eyes, which are not common signs parents will find alarming.

In a number of brain areas, neurons have been detected experimentally to enter into specific rhythmic patterns. The behaviors are characterized as spiking behavior, specifically spike wave discharges, spindles, and tonic spikes.

In all of these patterns, neuronal activity work in sequence to produce a large amplitude, a smaller amplitude oscilation, then another large amplitude (generally called bursting). Pressed between the alternating oscillations are distinct hyperpolarizations and depolarizations. This pattern continues until the seizure concludes which can be observed by inactive or at rest phases. Whereas spindles and tonic bursts are an extended sequence of alternating amplitudes.

The neuronal activity is from a multiple time scale drive-response mechanism which we credit to the thalamo-cortical basis model. Our goal is to specifically study a coupled Ordinary Differential Equation (ODE) thalamo-cortical model within a non directed graph network of 31 electrodes. We begin our study of with a single compartment model for frequency analysis, phase synchrony and then extend to 31-compartment model, along with sensitivity analysis for coupling coefficients and comparison of our model and real data.

The epilepsy data is from published data in Zhang a historical patient data from University of Texas Southwestern Medical Center. Infant patients in the neurology unit that were diagnosed with Type I Glucose Transport Deficiency Syndrome.

Our goal is complete the following in the proceeding chapters:

- Chapter 2: Introduce background information about the brain, G1D epilepsy, and general facts about EEG data.
- Chapter 3: A thorough study of thalamo-cortical modelling history, a brief summary of 4 neurological models, and details of how our model was formulated.
- Chapter 4: Local stability analysis of single-unit model for equilibrium in addition to identifying periodic behavior. Once acquiring the linearized system,

we evaluate the Jacobian and critical points to find the stability or lack thereof of each of the critical points. Our goal is further explore stability echange between the four neuronal populations that are responsible for the oscillatory behavior.

- Chapter 5: Sensativity analysis of coupled network regarding parameters values that directly affect spiking behaviour (SWD & spindles), interference terms, and phase synchrony. Specifically, a claim explaining the altered stability and delayed bifurcation due to coupling. Comparison between single unit and coupled units highlighting the specific values of correlation coefficents that are needed for the neuronal behavior stated above.
- Chapter 6: Phase synchrony - parameter values which cause synchronized activity or more stable activity (identify the synchronization index) in additon to finding the degree of synchrony of full model. Stability analysis of the full 31 compartment model regarding a specific parameter, and give general discussion
- Chapter 7: Compilation of information learned in previous chapters, stating highlights and limitations of our model built from data

CHAPTER 2

Neuroscience Preliminaries

2.1 Neurons

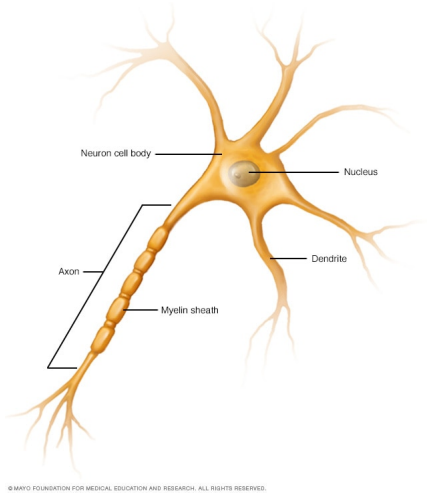

Figure 2.1: Basic Neuron, Medical Dictionary

There are approximately 100 billion neurons or nerve cells within the human brain. In addition to the neurons there are glia cells, which are also known as auxiliary cells, numbering up to 100 billion.

Each neuron may be connected to up to 10,000 other neurons, passing signals to each other via as many as 1,000 trillion synaptic connections. A classic example of a network, a neuron network correlated and coupled in a very complex way.

A neuron can be activated through electro-chemical signalling. Through this signalling, a neuron is able to communicate with up to several thousand neurons.

In this manner, the neurons pass signals through synapses. There are trillions of synaptic connections.

Before we begin a more global view of a neuron, it is useful to look locally first. More specifically, the neuron has 3 parts:

- Soma- cell body
- Dendrite- input, how a neuron receives information
- Axon- output, how a neuron sends information

Neurons contain mostly fluid and are surrounded by fluid. Dissolved in this water are ions such as sodium, potassium, chloride, and calcium. Each of these ions have a particular electrical charge. The ions pass from the soma to exterior of the cell through their perspective ion channel and then from the exterior to the soma. More explcitly, sodium channels only allows sodium to pass form the interior to exterior or exterior to interior. Additionally, this is true for chloride, potassium, and calcium.

The amount of ions in the extra cellular fluid is not exactly equal to the ion concentration within the cell. This is due to the cell membrane, not all ions are permeable and can pass through the membrane. Also, the cell membranes have pumps such as the sodium-potassium pump which removes sodium from the interior and adds in potassium to maintain equilibrium.

The difference between electrical potential within the cell and the exterior is referred to membrane potential, v. Hyperpolarization occurs when v is lowered or more negative and depolarization happens when v is increased and moves closer to 0. The neurons responsible for hyperpolarization and depolarization are also known as inhibitory and excitatory respectively, which we will often refer to throughout this document.

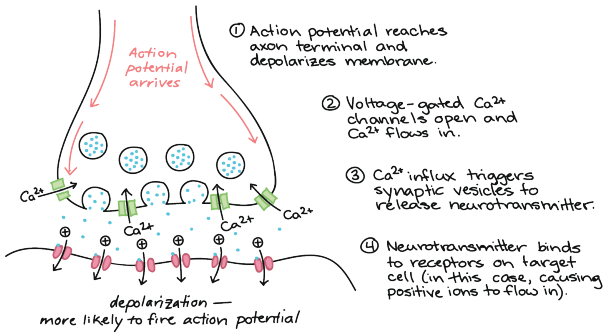

Figure 2.2: Synapse, Queensland Brain Institute

Back to the global view, a synapse is a junction by which a neuron sends information to another synapse. The synapse is a communication pass point. As stated above, neurons receive information when electrical and/or chemical signalling is obtained. There are two types of synapses. Electrical synapses send information by influx of ion channels, ions flow through the cell membranes. Where as chemical synapses, after successful action potential, the presynaptic neuron will send out or release neurotransmitters. Neurotransmitters are molecules, also known as chemical messengers, which travel to the target neuron and will either aid in a successful or unsuccessful action potential in the target neuron. Action potentials signify communication is present between neurons. If this does not happen, there is a breakdown at the synaptic level which is the basis of epilepsy.

2.2 Four types of Neuronal Populations

2.2.1 Pyramidal Neurons

Pyramidal neurons are commonly found in the cerebral cortex of every mammal. The name stems from the shape of the soma or cell body, it has a teardrop shape or a rounded pyramid form [9,12]. The physiological makeup consists of longer dendrites

protruding from the top end of the soma in addition to bundles of dendrites come out from the bottom end of the soma. Dendrites released from the top of the cell body are commonly referred to as apical dendrites whereas the the bundle of dendrites emerging from the bottom are called basal dendrites.

Pyramidal neurons are one of two dominant excitatory populations within the cerebral cortex. Pyramidal neurons release the neurotransmitter glutamate and number in size of about two-thirds of the total neuronal population in the cerebral cortex [9,11]. Their genetic makeup includes long axons that have capabilities of reaching as long as the spinal cord or outside of the brain. The importance of their makeup is tied to vital cognitive processes. These long axons may fail and become quite faulty which leads to brain disorders, epilepsy for example. Overly excessive excitation in particular brain regions containing intertwined pyramidal neurons is a clear marker for epilepsy.

2.2.2 Inhibitory Neurons

There are two main types of inhibitory neurons, Somatostatin and Parvalbumin, that work closely with excitatory neurons such as the pyramidal neurons by communicating with target neurons in the thalamus.

Somatostatin inhibitory neurons make up 50% of the inhibitory neuronal population in the cerebral cortex. Second most populous within the cortex. Somatostatin is a peptide hormone consisting of intracellular protein responsible for signalling more peptides and proteins. These neurons are present both in upper and deeper levels of the cerebral cortex, moreso in the upper levels. A somatostatin neurons axon can stretch horizontally over large regions. Their target neuron usually have distal dendrites in order to instill a delayed response to the target stimuli, hence the inhibitory name.

On the other hand, the Parvalbumin, is a calcium binding protein known to regulate ion channel flow. Parvalbumin inhibitory neurons makeup 40% of the interneuron subpopulations of the cerebral cortex. Interneurons are "middle man" neurons, they assist in communication from neuronal region to another distant region. Parvalbumin neurons are fast spiking neurons due to their extensive divisional skills. The most important effects of Parvalbumin neurons on the neuronal network are their short recovery time which leads to an increased rate of action potentials fired and secondly, their received input from excitatory neurons located in the thalamus. Input from the thalamus translates to a process called "fast feed forward inhibition" which is the inhibition of local excitatory neurons in a unidirectional manner [9]. Unidirectional inhibition is a process where excitatory neurons cannot excite the Parvalbumin neuron in response to the inhibition.

2.2.3 Specific Relay Nuclei

Specific Relay Nuclei are one of three types of thalamic nuclei. Relay nuclei receive very specific and defined input. The input is then projected as a signal to precise areas of the cerebral cortex with special functionalities [21]. Specific Relay Neuclei are mainly responsible for excitatory interaction with the cerebral cortex.

There are three varying types of nuclei. The first type are nuclei that relay or project signals for primary sensations. These include the ventral posterolateral nuclei that relay primary sensations known to represent majority of the primary somatosensory portion of the brain. Whereas the ventral posteromedial responsible for transferring sensory information from the face and oral cavities. Two other types of nuclei include the medial geniculate and the lateral geniculate, both responsible for attention spans (maintaining and directional) and main connection to optic nerves

and occipital lobe within the brain [22]. All of these connections are vital to painting the global picture of modality during an epileptic seizure.

The second type of nuclei give feedback from cerebellar signals, also known as the ventral lateral. Ventral Lateral nuclei receive input from the cerebellum and send signal to the primary motor cortex [23].

Lastly, the nuclei responsible for receiving feedback from the basal gangliar is known as the ventral anterior nucleus. Ventral Anterior nuclei send signals to the premotor cortex which allows for the establishment and follow through of movement in the body [24,25].

2.2.4 Thalamic Reticular Nucleus

The thalamic reticular nucleus is a collection of nerve cells specifically located in white matter of the thalamus, just between an internal capsule and external medullary lamina. Its main functionality includes facilitating communication between the thalamocortical and corticothalamic axons, the tie between the thalamus and cerebral cortex. All axons passing from the thalamus or the cortex must pass through this nucleus. The nucleus also receives GABA-ergic supplies from the axons passing through. These GABA-ergic supplies come in the form of glutamatergic afferents which are known to be excitatory [16].

According to much of the research literature related to rat brains similar to human brains, there are three types or functional modalities of Thalamic Reticular Necluei (TRN). Those modalities include: sensory, motor, and limbic. Sensory functionality allows for one to sense touch, skin stimulation (somatosensory), hear sounds (auditory), taste (gustatory), smell, have intellectual thoughts or emotions (visceral), or to see (visual). Motor function include movement of the bone structure

or skeletal system. Lastly, the limbic function modality stems from the thalamus and is responsible for how one feels emotions, memories, and stimulation or arousal.

Physicality of these type of nuclei include large cell bodies and varying axon lengths.

2.3 Epilepsy

Epilepsy is a neurological disorder where neuron activity is abnormal which causes seizures. The abnormal behavior is classically considered to originate from an "imbalance between excitation and inhibition in a localized region, multiple brain areas or the whole brain"[6]. Furthermore as described in animal models of epilepsy, epilepsy can be caused by persistent long-term alterations in death of presynaptic connections in addition to synaptic fluid-filled vacuole recycling.

For children, epileptic activity lies in the process of how the brain matures. A brain that is not fully formed or matured has the tendency to skew towards increased excitation, specifically mechanisms at the molecular level like the depolarization (increasingly non-negative voltage) of GABA and overly expressive NDMA (N-methyl-D-aspartate) receptors which are responsible for memory and learning impairments both cause excitation within the neuronal network.

G1D Transport Deficiency Epilepsy, also known as the GLUT1 Deficiency Syndrome, is a disorder which affects the nervous system. G1D is caused by mutations in the SLC2A1 gene. This gene gives instructions to produce a protein which is the glucose transporter protein type 1 (GLUT1). Most importantly, the GLUT1 protein moves glucose between glia (cells within the brain), which protect and maintain neurons. G1D can be identified by the high number of seizures during the infant stage which is usually rapid and irregular eye movement. Most notable visually recognized when and the point at which the size of the brain and skull both grow at a very

slow rate. As a result, the patient usually has a smaller head size, otherwise known as microcephaly. Due to microcephaly, G1D patients do experience developmental delays and mental/intellectual incapabilities.

Common Neurological issues:

- muscle tenseness which causes stiffness
- ataxia or complications with correlating body movements
- dysarthria which is speech difficulties
- lethargy
- headaches
- muscle twitches mainly during times of fasting
- confusion

GLUT1 then transports sugar into the cells from the blood or other cells to use as fuel. G1D is diagnosed through a blood test. GLUT1 is responsible for moving glucose around as the brain's main energy source, specifically within the blood-brain barrier, which gravely affects developmental growth.

According to the National Institute of Health, G1D is a very rare disorder. Only about 500 cases have been reported across the world since its discovery in 1991. Many researchers believe that this means the disorder is under diagnosed due to its similar symptoms to other neurological disorders.

2.4 Electroencephalogram (EEG)

According to Mayo Clinic, An electroencephalogram (EEG) is a test that detects electrical activity in the brain using small, flat metal discs (electrodes) attached to the scalp. Brain cells communicate via electrical impulses and remain active continuously, even during sleep.

The EEG measures voltage as neurons communicate through electrical impulses for any and every action the body makes. EEG is preferred over other methods such as functional magnetic emission imaging (fMRI) and positron emission tomography (PET) due to its portable ease, minimal invasiveness to the brain, but mostly the accurate temporal resolution. The exact time point of brain (neuronal) activity can be depicted by an EEG. Downfall of the EEG is that it cannot measure the specific neuron that is active at any particular time point nor can it provide a source activation pattern. The EEG only measures an average of voltage change of neurons depending on location of the electrode placed on the scalp, which is not precise enough to give information about one specific neuron.

2.5 EEG Brain Map

There are several detector distributions which depend on the number of probes of the EEG: 32 channels, 64 channels, 128 channels, 256 channels, etc. In this scenario, all patient data were obtained from a 32-channel electrode brain map. A Mitsar 32 Channel EEG Amplifier with WinEEG Software was used to record the data from G1D patients.

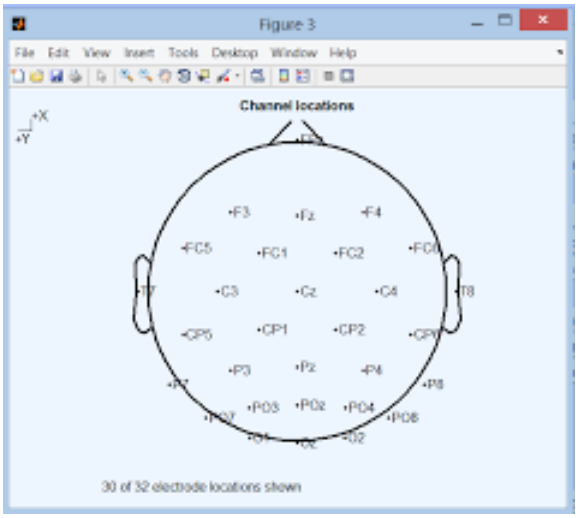

Figure 2.3: EEGLab 32 Electrode Map

2.6 Power Spectrum

The multi-step process of Power Spectrum strips away the noisy electrical activity within a brain in order to initiate neurological diagnosis and assist in the development of neurobiological instruments [40]. Many resarchers, biologists specifically, use this process in order to conduct frequency analysis during which the patient is asked to perform a visual task.

As stated before, EEG signals track the voltage fluctuations within the brain of a patient while completing a task. This task could be touching an item, signalling when a light has gone from off to on, writing, etc. For the purpose of this paper, we look for the neurological activity from a patient suffering from an epileptic seizure.

This process begins with a 32-channel EEG, active brain data is retrieved. First step is to remove unwanted noise signalling, a result of the EEG retrieving electrical activity from the scalp which could be from background tasks such as breathing, blinking, or other involuntary bodily movements. Frequency range during this step lies between 0.1-60 Hz. Signal preprocessing continues with manual dismission or

trimming of artifacts throughout the time length of the recorded signal. After the removal of the power line and lower level frequency artifacts, the frequency range is 0.1-50 Hz.

The third step concludes with an assortment of components as a result of Independent Component Analysis (ICA) of the 32 channels. Correlative information between the channels seen after this step is used to build the mathematical model seen in the next chapter. At this stage a wavelet transform or Fourier Analysis is used to process the signal into the various frequency bands,

- delta: 0-4 Hz
- theta: 4-8 Hz
- alpha: 8-13 Hz
- beta: 13-30 Hz

High power levels are observed in the delta and beta frequencies. The goal is to take the voltage trajectory into the frequency domain through Fourier Transforms and plot this information in the frequency domain.

Specifically for our research we find that important mechanisms, spiking neurons, are lost as a result of this transform. Our model has very rich nonlinear dynamics within the system which is why we chose to waive the power spectrum process.

2.7 Spiking Neurons Classifications

There are several spiking neurons classes. Most examples of spiking behavior are seen in healthy states or general resting state of a brain. First, we introduce spiking or busrting behavior seen in non-seizure or healthy states within the cortical region, also known as integrate and fire neurons[41]:

- Regular Spiking: Excitatory Neurons most commonly found in the cortex. In the case of extended stimuli, these neurons fire a small amount of spikes, a short

period in between spikes, followed by a continuous increase in period. This process is commonly known as spike frequency adaptation [41].

- Intrinsically Bursting: These excitatory neurons fire a conventional burst of spikes accompanied with continual singular spikes.
- Chattering: Excitatory neurons are capable of firing ceremonius bursts of tightly spaced spikes.
- Fast Spiking (Tonic Spiking): Inhibitory neurons which are capable of firing sequential periodical episodes of action potentials charateristically showing exceedingly high frequency, most commonly without any spike frequency adaptation which is defined by a slowing of frequency.
- Resonator: Neurons have diminished or continued below threshold oscillations.
- Low-Threshold Spiking: Inhibitory neurons known to have low firing threshholds. Conversely, these neurons also fire higher-frequency sequence of action potentials along with spike frequency adaptation.
- Thalamo-Cortical Oscillations: These neurons have two characteristics, if beginning at a resting state thalamo cortical neurons then exhibit a depolarization followed by tonic spiking. Yet if these neurons are hyperpolarized then they will fire or present a backlash emergence of action potentials.

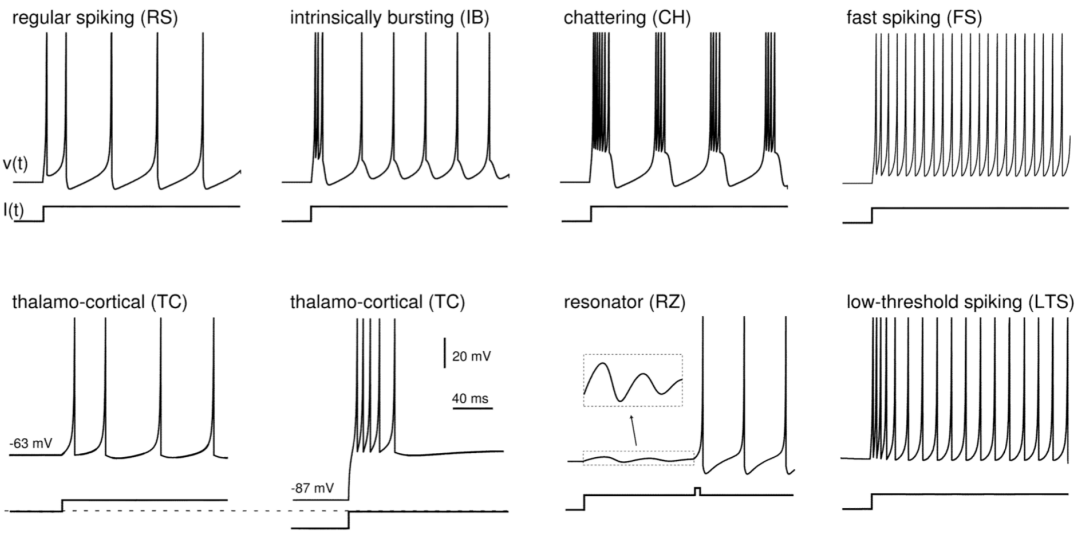

Figure 2.4: Eugene M. Izhikevich Model Spiking Neuron [41]

Spiking Neuron classification depends solely on the location of the neuron within the brain. As for G1D Transport Deficiency Epilepsy, the seizures are characterized closely to absence seizures. General seizures are indicated by specific spiking behavior. In this section we will also show examples of this activity. Chapter 4 shows actual behavior seen from our mathematical model. Disease state spiking behavior and subjects of our future studies are listed below:

- Spindles: Commonly reffered to as sleep spindles which are seen in stage 2 of non-REM (non- Rapid Eye Movement) sleep. Common indicator of onset of sleep, characterized by the two-step process. First step is a lessening spindle with a frequency 7-12 Hz followed by second step of periodic spindle episodes with slower frequency of 0.1- 0.2 Hz.
- Spike Wave Discharges: Characteristic of absence seizures, commonly seen on an EEG at a broad general frequency of 7-12 Hz. Researchers show that these neurons are thalamocortical oscillations.

- Slow Wave: An indicator of cerebral pathology or abnormal activity lying within the brain region beneath the EEG electrode. Many researchers brand this activity as "breach rhythm" (American Epilepsy Society).

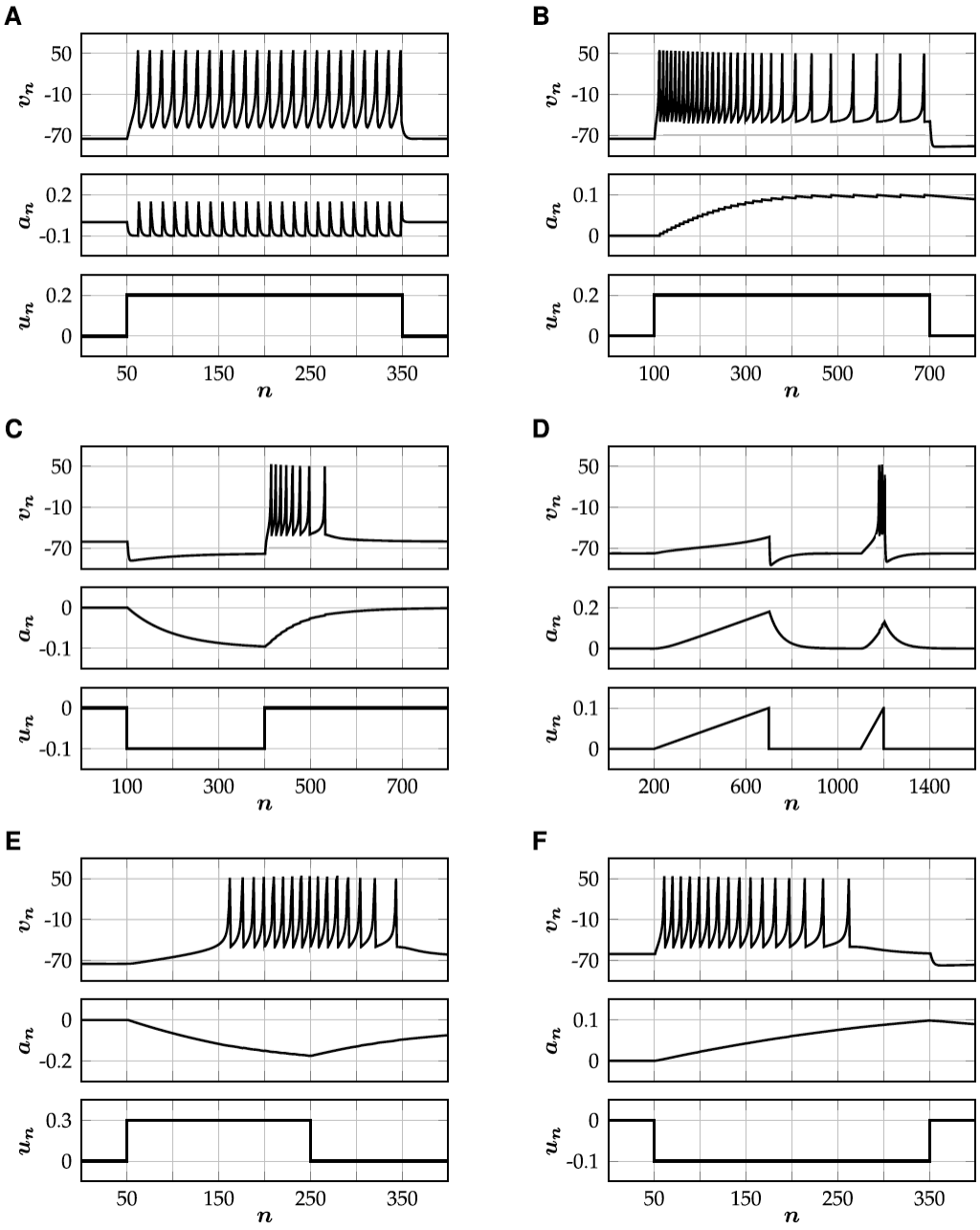

Figure 2.5: (a) Tonic Spiking (b) Spike Frequency Adaptation (c) Rebound Spiking (d) Accomadation (e) Spike Latency (f) Inhibition-influenced Spiking [41]

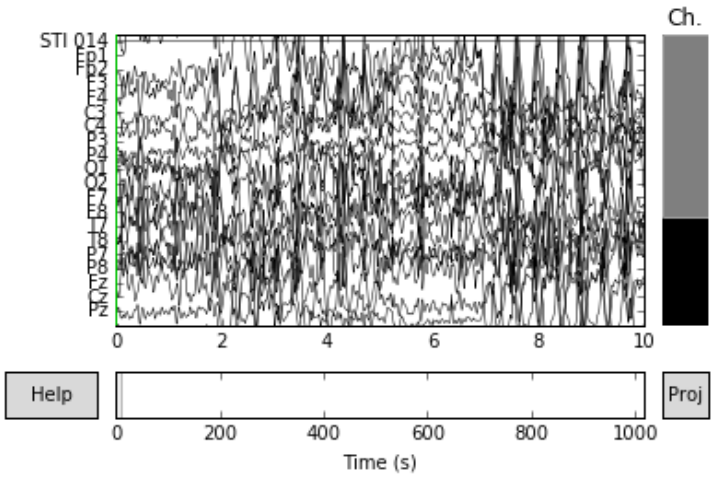

Figure 2.6: Source: Historical Patient data from Zhang [15], Slow Wave from Raw EEG signal output through MNE-Python Interface

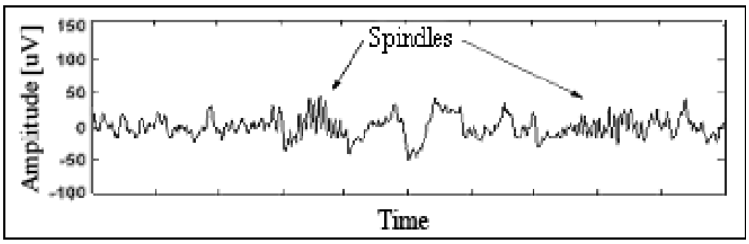

Figure 1. Example of sleep spindle in raw EEG signal [11]

Figure 2.7: Sleep spindles seen from EEG signals of Newborn Infants. Source: Bhattacharyya et. al, IEEE 2011 [43]

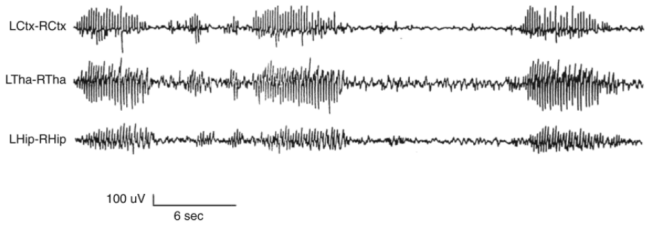

Figure 2.8: Spike Wave Discharges seen from an EEG of rats clinically altered to have absence seizures. Source: Pharmacologically Induced Animal Models of Absence Seizures

CHAPTER 3

Pre-Modeling the Neuronal Populations which Produce Epileptic Behavior of G1D

3.1 Thalamo-Cortical Modelling History

In this chapter, we will review the modelling history of thalamo-cortical based theory for epilepsy models.

3.1.1 Wilson-Cowan Model

The abnormal brain activity, characteristic of Epilepsy, as stated above is seen at the cellular level of brain rhythms through the use of an EEG. Just like the common cold, there are multiple types of Epilepsy. Yet most commonly, past literature has shown epileptic activity from the somatosensory or motor cortex. Wilson-Cowan (1972) first introduced a model showing the dynamics of a network of neurons consisting of excitatory and inhibitory neurons. A coupled nonlinear differential equations model produced to show the voltage changes seen from spatially localized excitatory and inhibitory neuronal populations.

Many, if not most, regions of the brain process large amounts of systematic input. In order to truly understand and visually represent the activity, researchers such as Ermentrout[31], found that tracking average firing rate within the neuronal networks is a more accurate model. This is the apporach Wilson-Cowan also took by using equations to mathematically model the cellular behavior of larger neuronal networks with underlying statistical processes.

Wilson-Cowan first began with a space-clamped model which was a set of integral equations particularly focused on the activity large network of tightly packed

coupled neuron cells over a fixed time frame. Specifically, two cell populations excitatory and inhibitory, $a_e(t)$ and $a_i(t)$ respectively. The duo found that these type of neurons cause their neighbor to be less active. To represent this phenomena over time, they used nonlinear activation functions, F_e and F_i. Depicted in the following equations:

$$\tau_e \frac{da_e}{dt} = -a_e(t) + [1 - r_e a_e(t)] F_e(w_{ee} a_e(t) - w_{ei} a_i(t) + I_e(t))$$
$$\tau_i \frac{da_i}{dt} = -a_i(t) + [1 - r_i a_i(t)] F_i(w_{ie} a_e(t) - w_{ii} a_i(t) + I_i(t))$$

The Wilson-Cowan Model is a first order kinetics model wtih two timescales, $\tau_{e,i}$, one for each neuronal population. Timescales have a direct proportional relationship which allows for continual adaptations according to the response from each of the various subpopulations. Usual practice is to have two nonlinearities, F_e, F_i, as sigmoidal functions: $F_{e,i}(x) = \frac{1}{1+e^{-\gamma_{e,i}(x-\theta_{e,i})}}$ where $\gamma_{e,i}$ is the gain or increase in voltage from reaching action potential and $\theta_{e,i}$ represents the threshold necessary to reach action potential for each population.

Argument x denotes a weighted sum of the ratio of active excitatory and inhibitory cell populations. The term $w_{jk} \geq 0$ corresponds to the connection intensity from cell k to cell j.

Whereas $1 - r_j a_j(t)$ depicts the in between stage of action potentials, Kilpatrick [33] referes to this time period as the refractory dynamics. This tracking function helps to regularly resize or scale the parameters within the nonlinearity, F_j, where $j = e, i$

Stability analysis of fixed points $(a_e(t), a_i(t))$ was done through phase plane diagrams. Wilson-Cowan found that there were two specific modes of behavior. First, coupling strength means intensity of the connection of the synapses between excitatory cells. Secondly, a weakly concentrated connection between inhibitory cells leads to

limit cycles. Limit cycle is biologically characterized by the clumping of a small set of excitatory cells alongside other cells which then leads to increased occurances of action potential. This behavior initiates the inhibitory cells to turn off or shut down all other cells, creating a cyclic pattern.

As a result, many researchers found that producing models with mutually inhibitory or mechanisms for oscillations within the neural populations, where each population is seen as a separate stimulus, imperative to understanding the neural mechanics of decision making and even perceptual rivalry.

Wilson-Cowan also produced a model with less assumptions, spacial structures of the synapses and external or interference terms were not considered in the first model. Which led them to produce:

$$\tau_e \frac{\partial a_e(x,t)}{dt} = -a_e(x,t) + [1 - r_e a_e(x,t)] F_e(w^*_{ee} a_e - w^*_{ie} a_i + I_e(x,t))$$
$$\tau_i \frac{\partial a_i(x,t)}{dt} = -a_i(x,t) + [1 - r_i a_i(x,t)] F_i(w^*_{ei} a_e - w^*_{ii} a_i + I_i(x,t))$$

where $w^*_{jk} a_k$ pertains to a convolution operator

$$w^*_{jk} a_k = \int_\Omega w_{jk}(x-y) a_k(y,t) dy \tag{3.1}$$

which is a representation of the drive response mechanism often seen within neuronal popultion. In this specific case, it is the drive from population k to population j at location x.

The weight function

$$w_{jk}(x-y) = k_{jk} e^{-(x-y)^2/\sigma_k^2} \tag{3.2}$$

is an example of a Gaussian equation used to exemplify the decomposition of connections within the cortex as a result of distance. These functions are well known to produce a bell shaped curve, in this case it is used to aide the drive-response between excitatory and inhibitory cell populations over the Ω domain of discretionary size.

3.1.2 Traub Model

Roger Traub and his colleagues set out to analyze a single column thalamocortical theory based model demonstrating oscillatory behavior within the gamma frequency, sleep spindles, and lastly bursts distinctive to epilepsy. Population dynamics related to specifc cells, assembled in the thalamocortical network, present information from several compartmentalized neruons. The firing behavior all relates back to Thalamocoritcal Relay cells, nucleus reticularis cells, and low threshold spiking neurons equipped with long apical dendrites.

Traub et. al had an overarching goal to understand the behavior or large networks of neurons which is how motor control, planning, language, sensory processes, etc. are accomplished for humans. Previous models worked with small cell counts whereas the Traub model works with several distict cell types and their perspective firing behaviors such as Regular spiking, fast rhythmic bursting, and intrinsic bursting. Due to the complexitiy of including the multiplicity of cell types, the Traub model can be applied to a large set of behaviors[25].

Interneuron rate functions shown below were used to show the dynamics of g_{Na}, $g_{K(DR)}$, and a lower threshold calcium conductance $g_{Ca(T)}$ (often seen as a regulatory current). These rate coefficients stem from various kinetics such as slower inactivation in the Thalamocortical relay cell.

$$m_\infty = 1.0/1.0 + exp[(-V - 52.0)/7.40]$$

$$h_\infty = 1.0/1.0 + exp[(V + 80.0)/5.0]$$

$$\tau_m = 1.0 + 0.33/exp[(V + 27.0)/10.0] + exp[(-V - 102.0)/15.0]$$

$$\tau_h = 28.3 + 0.33/exp[(V + 48.0)/4.0] + exp[(-V - 407.0)/50.0]$$

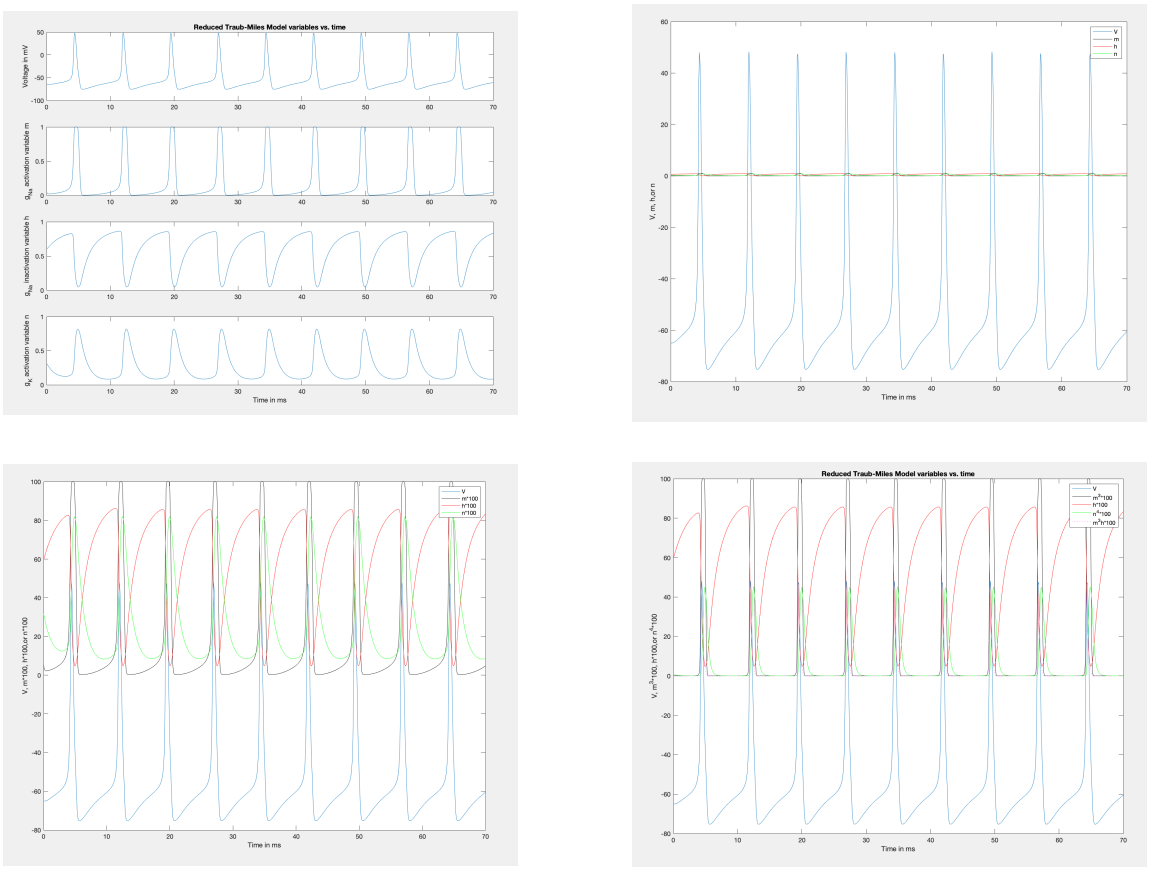

Figure 3.1: a) Traub Model: Resulting voltage with inactivation of two prevalent ion channels: g_{Na} and $g_{K(DR)}$b) Voltage of the full system and varying membrane potential for each ion channel (Sodium, Potassium, and Calcium) with increasing time. c)In depth view from figure 2.2, of the voltage behavior closer to 0. d)In order to undo the process that happens at 0 due to the gating variables only going from 0 to 1, voltage is then multiplied by a magnifiying constant.

Later, Traub and Miles [49] produced a reduced two-dimensional model which numerically examines a transition in I, current, through a critiacal value I_c. The Traub-Miles Model is based from Pyramidal Neuron in Rat Hippocamopus. Also known as the Reduced Traub-Miles Model is pre model of more complex model of a pyramidal excitatory cell in the rat hippocampus with respects to an Ermantrout and Kopell model [48].

$$\frac{dv}{dt} = \bar{g}_{Na}(m_\infty(v))^3(1-n)(v_{Na}-v) + \bar{g}_K N^4(v_K - v) + \bar{g}_L(v_L - v) + I, \tag{3.3}$$

$$\frac{dn}{dt} = \frac{n_\infty(v) - n}{\tau_n(v)} \tag{3.4}$$

In conclusion, the Traub model was still a global view of the intracellular workings of normal brain functionality. This model was a giant step forwad in the direction of considering the complexities of adding more cell types to a network model.

3.1.3 Taylor Model

Taylor et. al (2014) [38] then adapted the Wilson-Cowan model to epileptic seizures using a thalamo-cortical based theory. The Taylor model was produced to show that specific stimulations to model electrodes produces neuronal behavior called spike wave discharhges (SWD). Yielding SWD through two different paths, a thalamocortical connection and a corticocortical connection. This information lead to a Stochastic Differential Equation (SDE):

$$\frac{dPY(t)}{dt} = \tau_1(h_{py} - PY + C_1 f[PY] - C_3 f[IN] + C_9 f[TC]) \tag{3.5}$$

$$\frac{dIN(t)}{dt} = \tau_2(h_{in} - IN + C_2 f[PY]) \tag{3.6}$$

$$\frac{dTC(t)}{dt} = \tau_3(h_{tc} - TC - C_6(s[RE]) + C_7 f[PY])dt \tag{3.7}$$

$$\frac{dRE(t)}{dt} = \tau_4(h_{re} - RE - C_4(s[RE]) + C_5(s[TC]) + C_8 f[PY]) \tag{3.8}$$

Given that

$$f[u] = (1/(1+\epsilon^{-u})) \tag{3.9}$$

and

$$s[u] = au + b \tag{3.10}$$

is a sigmoidal function desgnating the slant of the sigmoid with variable ϵ.

Where $u = PY, IN, TC, RE$ where $i, j = 1, 2, ...19$.

Symbol	
PY	Pyramidal neural populations
IN	Inhibitory neural populations
$C_{1,\ldots,9}$	Connectivity parameters
A	Adjacency matrix
TC	excites PY populations
RE	activated by the TC neural populations

Table 3.1: Neurological Classes and Parameters

Taylor's main interest was to induce heterogeneaty into the system by incorporating behavior from various neuronal populations at distinct time steps but still keeping homogeneity within the time scales, $\tau_{1,2,3,4}$ and commencement parameters $h_{py,in,tc,re}$.

Due to the complexity of the system, the model solutions were computed with the use of Matlab's Euler-Maruyama solvers. Taylor then used a general Power Spectrum algorithm to obtain patient data with minimized noise. The patient data was then used to produce adjacent matrix A in the model above. Taylor et al. performed Pierson's Cross Correlation to gather information about associations between electrode channels. From the correlation matrix,

$$M_{i,j}=$$

$$\begin{cases} -M_{ij} & \text{if } M_{ij} < 0 \\ 0 & \text{if } M_{ij} < \lambda \\ \omega & \text{if } i = j \end{cases}$$

the Adjacent matrix is then calculuated,

$$A = \frac{1}{\sum_j M_{i,j}} M_{ij} \tag{3.11}$$

3.1.4 Fan Model

Fan et al. [37] projects that thalamic reticulus nuclei control spike wave discharges specifically in absence seizures. The model was further improved to incorporate time delay and other features. In Fan model, there are two main ways that the electrode units can be connected, in a straight line or a small world, connected with neighbors and small probability with distant nodes. The drive and response behavior can be seen in a unidirectional or bidirectional pattern.

Suczynski et al. (2004) [1] developed a computational model of thalamocortical circuits based on relevant (patho) physiological data. It was revealed that the interruption of the normal activity may be due to bistable dynamics consisting of background state and seizure rhythm. Lytton et al. (1997) [2] mainly focused on the thalamic TC-RE circuit in a computer network model of spike-and-wave seizures and showed that dynamic interactions determine partial thalamic latency. Taylor et al. (2014) [3] developed a thalamocortical neural field model, which can successfully simulate the SWD dynamics. Epilepsy regions are thought to be abnormally synchronized even between two remote seizure regions. However, these works mentioned above didn't model the distant cortical regions. In particular, they did not provide any insight into the synchronization dynamics of epileptic seizures. Therefore, based on the coupled thalamocortical models we reviewed the common mechanisms for the complete, lag and anticipated synchronization control, which are then tested for the efficacy of these mechanisms on the SWD synchronization. In particular, we investigated the motif synchronous dynamics of SWD. Such information provided insight for understanding how epileptic patients' brain network structure forms when the brain develops highly synchronous SWD during seizure.

Fan et al. discovered that in a two-compartment coupled thalamocortical model, there is sufficient evidence of complete synchronization with bidirectional coupling

where $x(t) = y(t)$, lag synchronization when there is a time lag introduced into the system $x(t) = y(t + \tau)$, lastly anticipated synchronization through active control methods [5]. In conclusion, based on SWD patterns from patient EEG, one can select relevant synchronization mechanism and network structure to model these brain activities and their collective behavior.

The model seen below considers the coupling effect with use of a sigmoidal function S, responsible for altering the mean membrane potential of the neuronal population into a mean pulse density of action potentials fired by the neurons [37]:

$$X'(t) = \alpha + AX(t) + F(X(t)) + K_1 S(Y_1(t)) \tag{3.12}$$

$$Y'(t) = \alpha + AY(t) + F(Y(t)) + K_1 S(X_1(t)) \tag{3.13}$$

where X_1, Y_1 are firing rates of the two neuronal populations from the cortex, X and thalamus, Y.

3.2 Problem Statement

In this current paper, our starting point is considering a real EEG taken from a patient with Glucose Transport Deficiency Type I Epilepsy (G1D). G1D is a genetic disorder where epilepsy is the main symptom along with microcephaly. G1D has a specific type of epilepsy where the patients suffer from absence seizures. We developed an ODE model adapted from the Taylor model mentioned above where we added in correlation coefficients and coupling strength terms. Our goal to understand how we can analyze G1D at a microscopic level from an EEG data set aiming to learn specific identifying characteristics due to its rarity and high risk of misdiagnosis. Finding a standard set of data patterns is quite complex. We strive to give the fundamental characteristics of data seen from EEG electrodes of a patient with G1D.

Clinically, researchers have found a way to produce imaging biomarkers of spike-and-wave discharges from patients with G1D by using fMRI informed EEG data (Vaudano et. al, 2016). In this case, with the use of EEG processing data, we extract a correlation matrix and base our equations within the thalamocortical model to give a visual of the neuronal behavior. Our model is bidirectional due to the correlation coefficients.

We want to study the EEG patterns to identify synchronization mechanisms of this brain disorder. Historically, all four neuronal populations communicate at different time scales which we propose aids in the distinct spiking neurons classes. nonlinearity. To verify our model, we will use EEG data from UT Southwestern to compare SWD and swindle neuronal behavior within real patient data given that an underdeveloped brain is reflected on EEG data. The motivation of this research is to find out how a neuron functions as a single unit with no inter-nueronal population coupling then simulate a small network of coupled electrodes with minimal coupling parameters followed by large coupling parameter, and lastly the full network with minimal and large coupling parameter. We will then use this information to analyze the self-interference terms within the behavior of the larger 32-electrode neuronal network.

3.3 Model Formulation

Building the mathematical model begins with the Taylor model as a basis then an added term representing the patient data, a very large and dense data set. We must first import patient data through an MNE-toolbox and Python interface, explained in further detail in the next section. From the Python interface we can produce a correlation matrix. Each network is built from previous knowledge of how

the four neuronal populations are intertwined. Which then leads to a branch point and node graph produced from common connections seen from correlation matrix.

From Chapter 2, we see how the neuronal activity continuously works within a network from the cerebral network and thalamus. There are two types of networks that we study, coupled and non-coupled in order to build a baseline of activity. We propose that there is unseen behavior with intercoupling terms from the cortex populations and thalamus populations in addition to separate intracoupling.

3.3.1 Pre-Seizure Data

Neuronal regions or electrodes will be used interchangeably as the electrodes represent a spatially localized neuronal region and not individual neurons.

Neurons form a large yet complex network. Before developing the mathematical model, we must first observe how the brain naturally communicates. Under the assumption of a seizure free state. The goal is to visualize how each neuron signals target specific areas elsewhere in the brain. A detection of activity is a pattern seen, specific to a patients brain during the resting or non-seizure state.

In Figure 2.1, a correlation matrix is shown. The correlation matrix, $A \in \mathbb{R}^{31\times 31}$ matrix where each element of the matrix is calculated by the measure of their linear dependence between the two values based from the Pearson Correlation equation.

$$\rho(X,Y) = \frac{1}{N-1}\sum_{i=1}^{N}(\frac{X_i-\mu_X}{\sigma_X})(\frac{Y_i-\mu_Y}{\sigma_Y}) \tag{3.14}$$

where $X = (X_i)$ and $Y = (Y_i)$ The value indicates the strength of the relationship, specifically $a(i,j)$ is the correlation between vector i and vector j. In our case, each vector represents average membrane voltage of a neuronal region recorded by the electrode over a period of time.

Symbol	
$\rho(X, Y)$	the correlation coefficient of the relationship between the variables X and Y
X_i	the values of the X-variable in column i
μ_X	mean of the values of the X-variable
σ_X	standard deviation of the values of the X-variable
Y_i	the values of the Y-variable in column i
μ_Y	mean of the values of the Y-variable
σ_Y	standard deviation of the values of the Y-variable
N	number of elements in each column

Table 3.2: Symbols used in Pearson Correlation equation

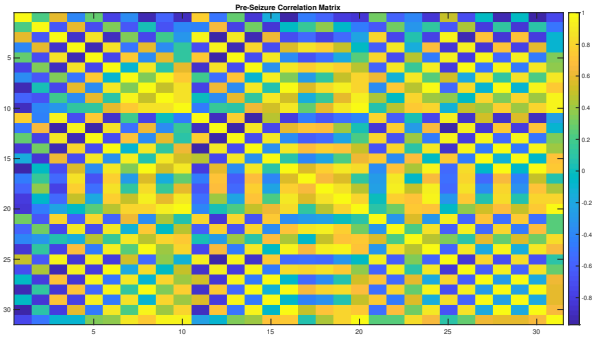

Figure 3.2: Pre-Seizure Correlation Plot

From this correlation matrix, we are able to see how each electrode is positively correlated by a value greater than 0 or negatively correlated, a value less than zero. We then can produce a network, starting with a data structure graph. In Figure 2.2, branch points and nodes diagram depicting how each electrode builds its network.

Each node represents an electrode or neuronal region. The branches form between each node if the correlation value $a(i, j)$ is greater than 0.6 or less than -0.6, our assumption is that electride i is highly positively or negatively correlated to electrode j, converse is true as well.

(a) Positive Correlation Graph (b) Negative Correlation Graph

Figure 3.3: Pre-Seizure Data Graph

On average, each electrode connects with 9.5 other electrodes in an excitatory fashion. On the other hand, an average of 5.8 inhibitory connections take place within this patients brain pre-seizure EEG data.

Looking further, regarding the postive correlation graph, there are several neuronal regions that are central to excitatory behavior:

Electrode: 11,25,13,15,7,31,10,30,6,24,26

In reality, electrodes $3, 4, 6, 8, 14, 20, 22, 24, 26, 27, 28, 29, 30, 31$ are the 14 electrodes whom have above average connections.

Wheras the graph for negative correlations is not as linear or uniform in pattern. In this case, electrodes $1, 2, 3, 4, 5, 6, 11, 12, 13, 14, 21, 22, 25, 26, 27, 28, 29$ are the 17 electrodes whom have above average connections. Furthermore, only 9 electrodes are well above average, meaning their number of connection is greater than the variance of the set of number of total connections. We use this information as a control. A way to compare brain activity at resting state to disease state.

3.3.2 Seizure Data

Viewing and understanding nueronal activity requires a more indepth, cellular exploration. Surface level brain activity patterns can be seen as a visual through an

EEG. Furthermore, neuronal region connections viewed are particularly random, one cannot accurately define an activation pattern from unpolished data.

Our overarching goal is to answer two questions:

1. What is phase synchrony?
2. Once a phase has been defined, how does one know that all channels are in synch?

Seizures are characterized by highly synchronized neuronal activity across the brain, in localized regions, or multiple spatially localized regions simultaneously connecting with other regions.

In order to see how the neurons build up their seizure network, we produced a correlation color plot. A spectral, visual representation of the correlation matrix. Correlation is a mutual relationship or connection between two or more neuronal regions. It shows the level of interdependence of variable quantities. In the figure below, we see the correlation color plot for the patient's seizure data.

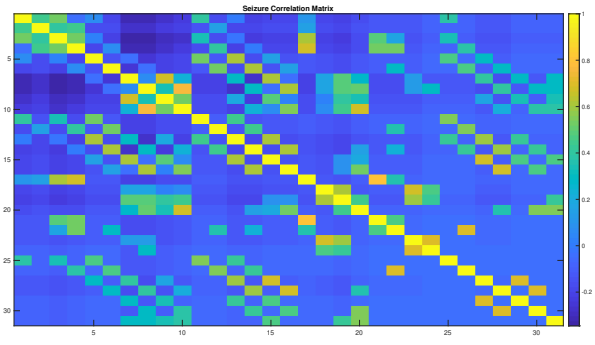

Figure 3.4: A Seizure Correlation Plot between 31 electrodes. Blue implies a strong negative correlation between two electrodes whereas yellow qualifies a strong positive correlation.

Two neuronal regions may work together to either inhibit or excite one another, producing an inhibitory relationship or an excitatory relationship. Voltage quantities for one region can increase otherwise known as depolarize and cause the other to decrease in voltage or hyperpolarize.

Figure 3.5: Seizure Data Graph: a) Positive Correlation Graph of 31 electrodes with connection strength $r_{x,y} \geq 0.6$. b)Negative Correlation Graph of 31 electrodes with connection strength $r_{x,y} \leq -0.6$

Brain activity during a seizure is seen to produce a different pattern compared to the pre-seizure graph. A general circular pattern is seen for the positive correlation graph. A natural assumption would be that this is an exact replica of approximate electrode locations on the scalp, yet this assumption is unrealistic.

On average each electrode connects with 7.2 other electrodes in an excitatory fashion. On the other hand, an average of only 2 inhibitory connections within a patients brain during a seizure. More specifically, regarding the postive correlation graph, there are two main poles. These poles cause a group of electrodes to congregate. This may indicate that these electrodes are more likely to cause excitatory behavior:

Left Hand Side Attractors: 7,8,9,10,15,19,20,23,29,31

Right Hand Side Attractors: 1,2,3,4,11,12,17,21,22,25

There are approximately 14 electrodes with above average number of connections. Electrodes: $3, 4, 6, 8, 14, 20, 22, 24, 26, 27, 28, 29, 30, 31$ have more than 7 total connections.

Wheras the graph for negative correlations has more of a oval or oblong shape with no attractors. Each electrodes appears to have similar connections in common. In this case, electrodes $1, 2, 3, 4, 5, 6, 11, 12, 13, 14, 21, 22, 25, 26, 27, 28, 29$ are the 17 electrodes with more than 2 connections. Which implies that the negative correlations are much lower in number. In biological terms, less inhibitory connections across the brain in an epileptic state. Looking even more in detail, only 9 electrodes are well above average, meaning their number of connections is greater than the variance of the number of total connections, which can be used as a threshold.

3.4 Summary of Results

In conclusion, we find that our graphs do give a useful visual as to how well the brain is connected in a healthy or non seizure activity. Yet it may not give an effective or accurate analysis of how synchronized various brain regions are connected before and during a seizure. Numbering the electrodes gives the reader a guantitative view of how the electrodes connect at one particular instant, in a healthy and unhealthy state. We look for most electrodes to have above average connections yet our goal would be to pinpoint more electrode connections made during a seizure. The reason for this occurance is the one timepoint considered rather than a fixed time period.

We gave an in depth quantitative view of the electrodes to:

- Find motifs seen by G1D based on circular or linear connections
- Pinpoint if these connections are due to symmetric coupling coefficients
- Determine symmetry in number of connections much like the correlation matrix. Why or why not does this symmetry replicate in the number of connections?

- State if we can visable see how the source pattern is connected from a graph or not.

The answers to these parenthetical thoughts and open ended questions will be found in our analysis of the full network model seen in Chapter 4 and 5.

CHAPTER 4

Modeling the Patterns of Epileptic Activity within a Network of Neurons Regarding G1D Transport Deficiency Epilepsy Seizures

The populations considered in this model represent neurons from two different parts of the human brain: Cerebral Cortex and Thalamus. We consider 4 specific populations consisting of the pyramidal nuerons, PY, the inhibitory neurons, IN, Specific relay neurons which represent the excitatory neurons in the Thalamus, SRN, and the thalamic reticular neurons which are the inhibitory neuronal population, TRN.

During an absence seizure, two parts of the brain, the cerebral cortex and the thalamus, coincide to produce certain neurological behavior. In order to mathematically represent the study of these complex processes during an epileptic seizure, various modeling assumptions will be instituted.

4.0.1 Modelling Assumptions

This model replicates a system of 31 electrodes from a 32-electrode EEG given a central electrode is used as a reference hence $j \in 1, 2, ..., 31$. We assume that neuronal activity never ceases. First, we begin with a single unit $j = 1$ then consider two-unit model analysis, $j = 1, 2$. The full network is analyzed in the next chapter.

Most of our model parameters stem from the induced epileptic spike wave discharge literature of Taylor et al. 2013, 2014, 2015; with adaptations from Fan et al. 2015; Wang et al. 2012 in addition to historical patient data. Much of the analytical

biological literature review gives biological functionality of the inter-compartment connections yet do not give exact parameter values.

We chose to analyze the coupled system across the thalamus and the cortex due to the fact that Fan mainly focused on the intraspective view of coupling, specifally looking at neurological activity of coupling within the cortex or within the thalamus, not a perspective of dynamics that can be seen from interspective coupling. Additionally, since we are modelling the coupling of nearby neuronal units or increased clustering, we do not consider a system of time delayed differential equations.

Symbol	
PY, IN, SRN, TRN	Firing rates (voltage)
$h_{p,i,t,r}$	additive input constants
	-0.35, -3.4, -2.0, -5
u_j	external control input into response module
	-0.3/-0.01, -0.3/-0.01, 0, 0
$\kappa_{1,2,3,4,5,6,7,8,9}$	connectivity strengths within different neuronal populations
	listed below
$sig_{PY,IN,SRN,TRN}$	activation functions for the cortical and thalamic modules
	$1/(1+250000^{-(u_j)})$
$\tau_{1,2,3,4}$	time scale parameters for each neuronal population
	26, 1.25*26, 26*0.1, 26*0.1
A	correlation matrix
s	approximation function

Table 4.1: Symbols and parameter values within G1D Model

In addition, in order to mimic the effect of stimulus-induced SWD, we performed a stimulus control $u_i(t)$ on the cortical variables, PY and IN, respectively, where $u_1(t)$ and $u_2(t)$ take the values in Table 1, and $(u_3(t), u_4(t)) = (0, 0)$. The control parameters are the same as those used in Taylor et al. (2014). During the simulations, k_6 is the bifurcation parameter which varies in the physiologically reasonable range, while the other parameter values are kept the same as the Taylor model.

$$\frac{dPY_j}{dt} = (h_p - PY_j + \kappa_1 sig(PY_j) - \kappa_2 sig(IN_j) + \kappa_3 sig(TRN_j))\tau_1 + \lambda_1 A(i,j) \tag{4.1}$$

$$\frac{dIN_j}{dt} = (h_i - IN_j + \kappa_4 sig(PY_j))\tau_2 \tag{4.2}$$

$$\frac{dSRN_j}{dt} = (h_t - SRN_j + \kappa_5 sig(PY_j) - \frac{\kappa_6}{2}(sTRN_j))\tau_3 + \lambda_2 A(i,j) \tag{4.3}$$

$$\frac{dTRN_j}{dt} = (h_r - TRN_j + \kappa_7 sig(PY_j) + \frac{\kappa_8}{2}(sSRN_j) - \frac{\kappa_9}{2}(sTRN_j))\tau_4 \tag{4.4}$$

Where:

Parameter	Origin	Target Area	Value
κ_1	PY	PY	1.8
κ_2	IN	PY	1.5
κ_3	SRN	PY	1
κ_4	PY	IN	4
κ_5	PY	SRN	3
κ_6	TRN	SRN	varying
κ_7	PY	TRN	3
κ_8	SRN	TRN	10.5
κ_9	TRN	TRN	0.2

Table 4.2: G1D Model Parameters [44]

We use sigmoidal (activation) functions to accurately simulate the action of the synaptic connections.

4.1 Find Equilibria and Existence

Let us begin with the 1-compartment model which has been dimensionalized. We see clearly that the trivial case of $E_0(0,0,0,0)$ is not an equilibrium point due to the fact that this implies the brain has no activity.

Therefore, we have the relation:

$$E_1(PY^*, IN^*, SRN^*, TRN^*) =$$

$$E_1([-\frac{0.96\lambda_1}{\tau_1} - \frac{(\kappa_1+\kappa_3)}{2} + \kappa_2\frac{IN^*+100}{200} - h_p - \frac{\kappa_3 TRN^*}{200}](\frac{200}{\kappa_1-200c_1}), \frac{h_i}{c_2} - \frac{\kappa_4}{c_2}(\frac{PY^*+100}{200}), [-\frac{0.96\lambda_1}{\tau_3} +$$

$$h_t + \kappa_5(\frac{PY^*+100}{200}) - \kappa_6(sTRN^* + \frac{1}{2})](\frac{1}{c_3}), (-\frac{1}{\tau_4(c_4+\frac{s\kappa_9}{2})})(h_r + \kappa_7(\frac{PY^*}{200} + \frac{1}{2}) + \frac{\kappa_8}{2}(sSRN^*)))$$

Which then becomes $D \cdot (PY^*, IN^*, SRN^*, TRN^*)^T = V$, in matrix form as:

$$D = \begin{pmatrix} (-c_1 + \frac{\kappa_1}{200})\tau_1 & -\frac{\kappa_2\tau_1}{200} & 0 & \frac{\kappa_3\tau_1}{200} \\ \frac{\kappa_4\tau_2}{200} & -c_2\tau_2 & 0 & 0 \\ \frac{\kappa_5\tau_3}{200} & 0 & -c_3\tau_3 & -\kappa_6 s\frac{\tau_3}{2} \\ \frac{\kappa_7\tau_4}{200} & 0 & \kappa_8 s\frac{\tau_4}{2} & (-c_4 - \kappa_9\frac{s}{2})\tau_3 \end{pmatrix}$$

set equal to:

$$V = \begin{pmatrix} (-h_p - \frac{\kappa_1}{2} + \frac{\kappa_2}{2} - \frac{\kappa_3}{2})\tau_1 - a_1\lambda_1 \\ -h_i\tau_2 - \frac{\kappa_4\tau_2}{2} \\ -h_t - \frac{\kappa_5\tau_3}{2} \\ -h_r - \frac{\kappa_7}{2} \end{pmatrix}$$

We then apply Cramer's Rule:

$$D_1 = \begin{pmatrix} (-h_p - \frac{\kappa_1}{2} + \frac{\kappa_2}{2} - \frac{\kappa_3}{2})\tau_1 - a_1\lambda_1 & -\frac{\kappa_2\tau_1}{200} & 0 & \frac{\kappa_3\tau_1}{200} \\ -h_i\tau_2 - \frac{\kappa_4\tau_2}{2} & -c_2\tau_2 & 0 & 0 \\ -h_t - \frac{\kappa_5\tau_3}{2} & 0 & -c_3\tau_3 & -\kappa_6 s\frac{\tau_3}{2} \\ -h_r - \frac{\kappa_7}{2} & 0 & \kappa_8 s\frac{\tau_4}{2} & (-c_4 - \kappa_9\frac{s}{2})\tau_3 \end{pmatrix}$$

$$D_2 = \begin{pmatrix} (-c_1 + \frac{\kappa_1}{200})\tau_1 & (-h_p - \frac{\kappa_1}{2} + \frac{\kappa_2}{2} - \frac{\kappa_3}{2})\tau_1 - a_1\lambda_1 & 0 & \frac{\kappa_3\tau_1}{200} \\ \frac{\kappa_4\tau_2}{200} & -h_i\tau_2 - \frac{\kappa_4\tau_2}{2} & 0 & 0 \\ \frac{\kappa_5\tau_3}{200} & -h_t - \frac{\kappa_5\tau_3}{2} & -c_3\tau_3 & -\kappa_6 s\frac{\tau_3}{2} \\ \frac{\kappa_7\tau_4}{200} & -h_r - \frac{\kappa_7}{2} & \kappa_8 s\frac{\tau_4}{2} & (-c_4 - \kappa_9\frac{s}{2})\tau_3 \end{pmatrix}$$

$$D_3 = \begin{pmatrix} (-c_1 + \frac{\kappa_1}{200})\tau_1 & -\frac{\kappa_2\tau_1}{200} & (-h_p - \frac{\kappa_1}{2} + \frac{\kappa_2}{2} - \frac{\kappa_3}{2})\tau_1 - a_1\lambda_1 & \frac{\kappa_3\tau_1}{200} \\ \frac{\kappa_4\tau_2}{200} & -c_2\tau_2 & -h_i\tau_2 - \frac{\kappa_4\tau_2}{2} & 0 \\ \frac{\kappa_5\tau_3}{200} & 0 & -h_t - \frac{\kappa_5\tau_3}{2} & -\kappa_6 s\frac{\tau_3}{2} \\ \frac{\kappa_7\tau_4}{200} & 0 & -h_r - \frac{\kappa_7}{2} & (-c_4 - \kappa_9\frac{s}{2})\tau_3 \end{pmatrix}$$

$$D_4 = \begin{pmatrix} (-c_1 + \frac{\kappa_1}{200})\tau_1 & -\frac{\kappa_2\tau_1}{200} & 0 & (-h_p - \frac{\kappa_1}{2} + \frac{\kappa_2}{2} - \frac{\kappa_3}{2})\tau_1 - a_1\lambda_1 \\ \frac{\kappa_4\tau_2}{200} & -c_2\tau_2 & 0 & -h_i\tau_2 - \frac{\kappa_4\tau_2}{2} \\ \frac{\kappa_5\tau_3}{200} & 0 & -c_3\tau_3 & -h_t - \frac{\kappa_5\tau_3}{2} \\ \frac{\kappa_7\tau_4}{200} & 0 & \kappa_8 s\frac{\tau_4}{2} & -h_r - \frac{\kappa_7}{2} \end{pmatrix}$$

Through Cramer's Rule, we find that the relation above leads to:

$\mathrm{PY}^* = \frac{detD_1}{detD}, IN^* = \frac{detD_2}{detD}, SRN^* = \frac{detD_3}{detD}, TRN^* = \frac{detD_4}{detD}$[1]

Theorem 4.1.1. *If $Det(D) \neq 0$, then there exists one unique equilibrium of the linearized one-compartment Taylor Model.*

4.2 Local Stability Analysis

4.2.1 Single Unit Analysis

The Jacobian matrix without correlation constant is

$$J = \begin{pmatrix} (-c_1 + \frac{\kappa_1}{200})\tau_1 & -\frac{\kappa_2\tau_1}{200} & 0 & \frac{\kappa_3\tau_1}{200} \\ \frac{\kappa_4\tau_2}{200} & -c_2\tau_2 & 0 & 0 \\ \frac{\kappa_5\tau_3}{200} & 0 & -c_3\tau_3 & -\kappa_6 s c_4\tau_3 \\ \frac{\kappa_7\tau_4}{200} & 0 & -\kappa_8 s c_3\tau_4 & (-c_4 - \kappa_9 s c_4)\tau_4 \end{pmatrix}$$

We then evaluate the Jacobian at the single equilibrium point for the 1-compartment model. The Jacobian evaluated at $E_1([-\frac{0.96\lambda_1}{\tau_1} - \frac{(\kappa_1+\kappa_3)}{2} + \kappa_2\frac{IN^*+100}{200} -$

[1]Equilibrium relation espression is available upon request

$h_p - \frac{\kappa_3 TRN^*}{200}](\frac{200}{\kappa_1 - 200c_1}), \frac{h_i}{c_2} - \frac{\kappa_4}{c_2}(\frac{PY^*+100}{200}), [-\frac{0.96\lambda_1}{\tau_3} + h_t + \kappa_5(\frac{PY^*+100}{200}) - \kappa_6(sTRN^* + \frac{1}{2})](\frac{1}{c_3}), (-\frac{1}{\tau_4(c_4 + \frac{s\kappa_9}{2})})(h_r + \kappa_7(\frac{PY^*}{200} + \frac{1}{2}) + \frac{\kappa_8}{2}(sSRN^*)))$ is

$$J(E_1) = \begin{pmatrix} (-c_1 + \frac{\kappa_1}{200})\tau_1 & -\frac{\kappa_2\tau_1}{200} & 0 & \frac{\kappa_3\tau_1}{200} \\ \frac{\kappa_4\tau_2}{200} & -c_2\tau_2 & 0 & 0 \\ \frac{\kappa_5\tau_3}{200} & 0 & -c_3\tau_3 & -\kappa_6 s c_4 \tau_3 \\ \frac{\kappa_7\tau_4}{200} & 0 & -\kappa_8 s c_3 \tau_4 & (-c_4 - \kappa_9 s c_4)\tau_4 \end{pmatrix}$$

The Jacobian is unchanging due to the system being linear. Hence the characteristic polynomial $P(\lambda) = det(\lambda I - J)$ can be calculated as $P(\lambda) = \lambda^4 + (c_2\tau_2 + c_3 t_3 + c_1\tau_1 - \frac{\kappa_1\tau_1}{200} + c_4\tau_4 + c_4\kappa_9 s\tau_4)\lambda^3 + (\frac{\kappa_4\kappa_2\tau_2\tau_1}{40000} + c_1c_4\tau_1\tau_4 - \frac{c_4\kappa_1\tau_1\tau_4}{200} - \frac{\kappa_3\kappa_7\tau_1\tau_4}{40000} + c_1c_4\kappa_9 s\tau_1\tau_4 - \frac{c_4\kappa_1\kappa_9 s\tau_1\tau_4}{200} + (c_2\tau_2 + c_2\tau_3)(c_1\tau_1 - \frac{\kappa_1\tau_1}{200} + c_4\tau_4 + c_4\kappa_9 s\tau_4) + c_2c_3t_2t_3 + (\kappa_8 c_3 s\tau_4)(c_4\kappa_6 s\tau_3))\lambda^2 + ((\frac{\kappa_4\kappa_2\tau_2\tau_1}{40000})(c_3\tau_3 + c_4t_4 + \kappa_9 s c_4\tau_4) + (c_2c_3\tau_2\tau_4)(c_1\tau_1 - \frac{\kappa_1\tau_1}{200} + c_4\tau_4 + c_4\kappa_9 s\tau_4) + (\kappa_8 c_3 s\tau_4)(-\frac{\kappa_3\kappa_5\tau_1\tau_2}{40000} + c_1c_4\kappa_6 s\tau_1\tau_3 - \frac{c_4\kappa_1\kappa_6 s\tau_1\tau_3}{200}) + (c_2\tau_2\kappa_8 c_3 s\tau_4)(c_4\kappa_6 s\tau_3))\lambda + (\frac{\kappa_2\kappa_4\tau_1\tau_2}{40000})(c_3\tau_3c_4\tau_4 + c_3\tau_3\kappa_9 s c_4\tau_4 + \kappa_8 s^2 c_3\tau_4\kappa_6 c_4\tau_3) + (c_2c_3\tau_2\tau_3)(c_1c_4\tau_1\tau_4 - \frac{c_4\kappa_1\kappa_6 s\tau_1\tau_3}{200}) + (c_2c_3\kappa_8 s\tau_2\tau_4)(-\frac{\kappa_2\kappa_4\tau_1\tau_2}{40000} + c_1c_4\kappa_6 s\tau_1\tau_3 - \frac{c_4\kappa_1\kappa_6 s\tau_1\tau_3}{200})$. To solve this fourth order characteristic polynomial, it is simpler to solve in terms of c_1, c_2, c_3, c_4, the inference terms. We then consider 4 cases:

Case 1: Let $c_1 = c_2 = c_3 = c_4 = 0$. The eigenvalues are $\lambda_1 = 0$, $\lambda_2 = 0$, $\lambda_3 = \frac{117 - \sqrt{668759}}{1000} < 0$, $\lambda_4 = \frac{\sqrt{668759} + 117}{1000} > 0$

Case 2: Let $c_1 = c_2 = c_3 = c_4 = 1$. The eigenvalues are $\lambda_1 = -3.3267 + 25.8285i$, $\lambda_2 = -3.3267 - 25.8285i$, $\lambda_3 = -24.6472 + 0.000i$, $\lambda_4 = -33.6214 + 0.000i$

Case 3: Let $c_1 = c_3 = 0$ and $c_2 = c_4 = 1$. The eigenvalues are $\lambda_1 = 0$, $\lambda_2 = -32.1793$, $\lambda_3 = -4.1388$, $\lambda_4 = -0.0039$

Case 4: Let $c_1 = c_3 = 1$ and $c_2 = c_4 = 0$. The eigenvalues are $\lambda_1 = 0$, $\lambda_2 = -28.3561$, $\lambda_3 = -0.404$, $\lambda_4 = 0.3941$

Hence E_1 is Locally Asymptotically Stable only in Case 4 where $c_1 = c_2 = c_3 = c_4 = 1$.

For general stability we the considered the 4D Routh-Hurwitz Criterion: $a_0 > 0$, $a_1 > 0$, $a_1a_2 - a_0a_3 > 0$, $a_1a_2a_3 - a_1^2a_4 - a_0a_3^2 > 0$, and $a_4 > 0$ for $P(\lambda) = a_0\lambda^4 + a_1\lambda^3 + a_2\lambda^2 + a_3\lambda + a_4 = 0$.[2] We primarily consider the stability with respects to c_i to support a claim stated in the next chapter.

Considering actual values used in simulations for each of the parameters as listed in Table 4.2, our Jacobian Matrix then simplified to:

$$J = \begin{pmatrix} (-26(0.009 + c_1) & -0.195 & 0 & \frac{13}{100} \\ 0.65 & -32.5c_2 & 0 & 0 \\ 0.039 & 0 & -2.6c_3 & -8.6268c_4 \\ 0.039 & 0 & 76.44c_3 & -4.056c_4 \end{pmatrix}$$

which then lead to the following characteristic equation:

$P(\lambda) = 2.6c_3\lambda^3 + (0.7352 + 84.5c_2c_3 - 67.6c_1c_3 - 10.53c_3c_4)\lambda^2 + (0.3296c_3 + 345.7138c_4 + 2197c_1c_2c_3 - 274.1856c_1c_4 - 19.773c_2c_3 + 659.3714c_3c_4)\lambda + 8911.032c_1c_2c_3c_4 - 69.3875c_3c_4 - 80.1993c_4 + 17145.2474c_1c_3c_4 - 0.3876c_3$

Theorem 4.2.1 (Routh-Hurwitz)**.** *The roots of the auxiliary equation have negative real parts if and only if all the principal diagonal minors of the Hurwitz matrix are positive provided that* $a_0 > 0 : \delta_1 > 0, \delta_2 > 0, ..., \delta_n > 0$. *As* $\delta_n = a_n\delta_{n-1}$, *the last inequality can be written as* $a_n > 0$.

[2]see Appendix A for Routh Hurwitz stability criterion of single compartment without correlation constant and eigenvalues.

Using Routh-Hurwitz, stability criterion can be determined by, given the characteristic polynomial with degree $n = 3$ of form, $P(\lambda) = \lambda^3 + a_1\lambda^2 + a_2\lambda + a_3$, where $a_1 > 0$, $a_3 > 0$, and $a_1a_2 > a_3$ implies stability.

4.2.2 Plotting Stability Regions

We then used this criterion to find the 3 specific instances and the overlapping parameter space,

- $a_1 > 0$ yields $\frac{0.7352-67.6c_1c_3}{-2.6c_3} > 0$,
- $a_3 > 0$ yields $a_3 = 0.14907692 > 0$,
- $a_1a_2 > a_3$ yields $\frac{-0.12676923(0.7352-67.6c_1c_3)}{-2.6c_3} > 0.149077$.

These criterion came as a result of assuming the interference term coefficient is either on or off. Explcicitly stating, c_2 and c_4 were set equal to 0 so that we could interpret brain activity from the two most active brain areas, pyramidal nuerons and thalamic reticular nuclei neurons - our main dimensionalization tool.

We see in Figure 3.1, that the overlapping parameter space coincides with where $a_3 > 0$, labelled as data 3 in Figure 3.1.

4.3 Summary of Results

In this chapter, a full G1D model with correlation constants and coupling terms stemming from patient data has been presented. We considered plausible dynamics without explicit values for patient data and arbitrary coupling strenght values. This model was formulated to gain a better understanding of how self-interference terms, c_i, inhibitory in nature to its perspective neuronal population, alter stability. Stability analysis has shown that as the values of c_i range from 0 to 1, instability occurs in all scenarios. Two cases representing the dulling of inhibitory relations from the larger excitatory neuronal populations, pyramidal neurons and specific relay nuclei.

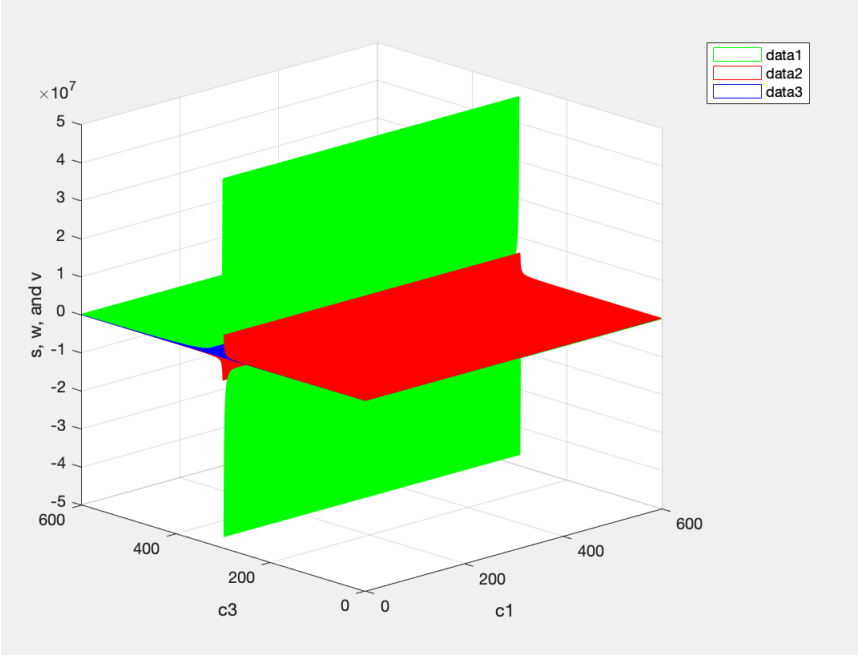

Figure 4.1: Single Unit Parameter Space

Whereas the other two cases denote a muting of excitatory dealings from the inhibitory populations, inhibitory neurons and thalamic reticular nucleus. Only in case 2 did we find a local asymptotically stable critical point. Furthermore, it can be seen that altering the values of self-interference terms leads to instability. This result would arguably lead to interesting dynamics in simulations, which is further explored in chapter 4.

CHAPTER 5

Coupled Network Simulations and Results

In the previous two chapters, we discussed stability regarding interference terms, patient data, and coupling coefficents of a one unit model. This chapter will continue to provide analysis for coupled two-unit model.

We use MATLAB ODE45 solver to nuerically solve and plot the solutions to the system of ODEs. ODE45 is an efficient way to solve non-stiff equations with medium accuracy in less than 1 minute.

5.1 Reasoning for Hopf Bifurcation and Assumptions

First, we begin wtih concretely explaining why there are spiking behavior changes in addition to a time delayed bifurcation between the single compartment and two-unit model as a result of increasing coupling strength. Our claim is that this will be a plausible way of behavior modulation in the fully coupled 31-unit system. We first study how 2 coupled units change stability.

Our claim:

Claim: Assume the self interference terms in each of the four neuronal populations, c_1, c_2, c_3, c_4, are arbitrary. We express each unit $(PY_j, IN_j, SRN_j, TRN_j)^T = X_1$ and $(PY_i, IN_i, SRN_i, TRN_i)^T = X_2$.

$$
\begin{aligned}
\frac{dPY_j}{dt} &= (h_p - c_1 PY_j + \kappa_1 sig(PY_j) - \kappa_2 sig(IN_j) + \kappa_3 sig(TC_j))\tau_1 + \lambda_1 \alpha_1 SRN_i + \alpha_2 TRN_i \\
\frac{dIN_j}{dt} &= (h_i - c_2 IN_j + \kappa_4 sig(PY_j))\tau_2 \qquad (\star) \\
\frac{dSRN_j}{dt} &= (h_t - c_3 SRN_j + \kappa_5 sig(PY_j) - \frac{\kappa_6}{2}(sTRN_i))\tau_3 + \lambda_2 \alpha_3 PY_i + \alpha_4 IN_i \\
\frac{dTRN_j}{dt} &= (h_r - c_4 TRN_j + \kappa_7 sig(PY_j) + \frac{\kappa_8}{2}(sSRN_j) - \frac{\kappa_9}{2}(sTRN_j))\tau_4
\end{aligned}
$$

Proof: Given two correlation matrices, G and M, which are square symmetric matrices, representing coupling coefficients within units and between units respectively (*) with $x_1 = X_1 - X_1^*$, $x_2 = X_2 - X_2^*$, by difference away from equilibrium. Therefore the homogenous system can be represented as:

$$x_1' = Gx_1 + Mx_2 \tag{5.1}$$

$$x_2' = Gx_2 + Mx_1 \tag{5.2}$$

Equations 5.1-2 then yield the following coefficient matrix:

$$A = \begin{bmatrix} G & M \\ M & G \end{bmatrix}.$$

To find the eigenvalues we then compute $|A - \lambda I|$

$$det(A - \lambda I) = \begin{pmatrix} G - \lambda I & M \\ M & G - \lambda I \end{pmatrix}.$$

It is given that for non-singular A_1

$$
\begin{aligned}
det \begin{pmatrix} A_1 & B_1 \\ B_1 & A_1 \end{pmatrix} &= det \left(\begin{bmatrix} A_1 & 0 \\ 0 & I \end{bmatrix} \begin{bmatrix} A_1^{-1} & 0 \\ 0 & I \end{bmatrix} \begin{bmatrix} A_1 & B_1 \\ B_1 & A_1 \end{bmatrix} \right) \\
&= det \left(\begin{bmatrix} A_1 & 0 \\ 0 & I \end{bmatrix} \begin{bmatrix} I & A_1^{-1} B_1 \\ B_1 & A_1 \end{bmatrix} \right),
\end{aligned}
$$

and if $A = XYZ$ then $detA = detXdetYdetZ$.

Without loss of generality:

$$\begin{bmatrix} G-\lambda I & M \\ M & G-\lambda I \end{bmatrix} = \begin{bmatrix} G-\lambda I & 0 \\ 0 & I \end{bmatrix} \begin{bmatrix} (G-\lambda I)^{-1} & 0 \\ 0 & I \end{bmatrix} \begin{bmatrix} G-\lambda I & M \\ M & G-\lambda I \end{bmatrix}$$

By Gaussian elimination,

$$\begin{aligned} detA &= det(G-\lambda I)\cdot det \begin{vmatrix} I & (G-\lambda I)^{-1}M \\ M & G-\lambda I \end{vmatrix} \\ &= det(G-\lambda I)\cdot det \begin{vmatrix} I & (G-\lambda I)^{-1}M \\ 0 & (G-\lambda I)-M^{-1}(G-\lambda I)^{-1}M \end{vmatrix} \\ &= det(G-\lambda I)\cdot det((G-\lambda I)-M^{-1}(G-\lambda I)^{-1}M) \\ &= det((G-\lambda I)^2-(G-\lambda I)M^{-1}(G-\lambda I)^{-1}M) \end{aligned}$$

Assume here $M = \gamma I$ as a special case and $a \pm ib$ are eigenvalues of G then

$$detA = ((\lambda - a) + ib)^2((\lambda - a) - ib)^2 - \gamma^2.$$

5.2 Effect of Coupling on Stability and Delayed Bifurcation

We assume for now $M = \mu I$ where I is the Identity matrix and μ represents coupling strength and consider G is near a Hopf-Bifurcation point at $k_6 = k_B$. There exists $Q(k_6)$ nonsingular matrix such that

$$\mathrm{Q}^{-1}GQ = det \begin{pmatrix} \lambda-(a+ib) & 0 \\ 0 & \lambda-(a-ib) \end{pmatrix}$$

for the projection to the largetst two eigenvectors and eigenvalues.

Hence,

$$det((G-\lambda I)^2-\mu^2 I) = det(Q^{-1}((G-\lambda I)^2-\mu^2 I)Q)$$
$$= ((\lambda-a)^2+b^2)^2-\mu^2$$

At, $k_6 = k_B$ (bifurcation point),

$$Re(a \pm ib) = a(k_6)\Big|_{k_6=k_B} = 0$$
$$Im(a \pm ib) = b(k_6)\Big|_{k_6=k_B} \neq 0$$

for the original Taylor Model.

As for the Two-unit coupled Model, the eigenvalues are

$$\lambda_{1,2} = a \pm ib - \mu,$$
$$\lambda_{3,4} = a \pm ib + \mu.$$

We observe the stability change prior to $k_6 = k_B$ due to $\lambda_{3,4}$ becomes positive before $k_6 = k_B$. We then investigate further the stability change due to coupling in the next section.

5.2.1 Impact on Stability by Coupling

Without coupling, the steady state changes from stable to unstable as real part of eigenvalues in the following way:

$$a(k_6) < 0 \text{ for } k_6 < k_B$$
$$a(k_6) > 0 \text{ for } k_6 > k_B$$

However, with coupling, $Re(\lambda_{3,4})$ becomes positive when $a(k_6)+\mu > 0$. Depending on the strenght of couplint, the stability exchange occurs before the bifurcation point k_B.

5.2.2 Impact on Delayed Stability by Coupling

For many neuronal systems discussed earlier in chapter 2, passage through delayed Hopf-bifurcation is an important rythmetic feature, as seen in many papers existing in literature.

In summary, as the parameter $k_6 = k_{6i} + \epsilon t$ where k_{6i} is the initial parameter, is slowly increasing, and if the solution

$$(PY_j, IN_j, SRN_j, TRN_j)\Big|_{t=0} = (PY^*, IN^*, SRN^*, TRN^*)$$

then Equations 4.1-4.4 bifurcates at a point beyond the original Hopf-bifurcation point at k_6^* which satisfies

$$\int_{k_{6i}}^{k_6^*} Re\lambda_{1,2}(\tau) = \int_{k_{6i}}^{k_6^*} a(\tau)d\tau = 0$$

where $k_6^* > k_B$ is beyond the Hopf-bifurcation point.

We consider the goverening Equations 5.1-5.4 and with coupling, the concerned eigenvalue condition will be

$$\int_{k_{6i}}^{k_6^{**}} Re\lambda_{3,4}(\tau) = \int_{k_{6i}}^{k_6^{**}} (a(\tau) + \sigma)d\tau = 0$$

and we expect an early bifurcation point than k^**_6. When σ is small but greater than 0, then $k_6^{**} - k_6^* = O(\sigma)$. We observed this important change of dynamics in our coupled system, as shown in the examples below.

5.3 Stability Analysis Regarding Parameter k_6

Through extensive simulations and data analysis, Fan [38,39], projects that k_6 is the key parameter that alters stability for a model of this sort. We completed stability analysis with the use of MATLAB and also found that within the full network system, k_6 is still a key parameter even with the addition of patient data and a coupling strength term. We solve our system of ODEs based from EEG data with MATLAB

ODE45 which then simulates the brain rhythms during an epileptic seizure within four minutes.

In this section, a comparison of the single compartment model to the two-coupled units model with increasing k_6 is computed. Figures below show the difference in behavior as k_6 increases from 4 to 5, moving through a suspected bifurcation point at $k_6 = 4.1$.

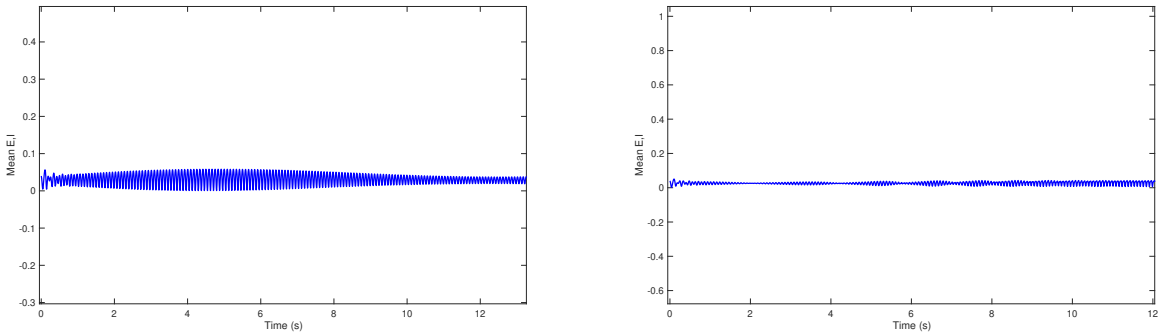

Figure 5.1: Hopf-bifurcation point beginning at $k_6 = 4$ and increasing to $k_6 = 5$ and $t = 0 - 12$s. A comparison of one unit model (left) to two-unit coupling model (right) showing small oscillatory spiking in the single compartment model versus little to no activity in the coupling model.

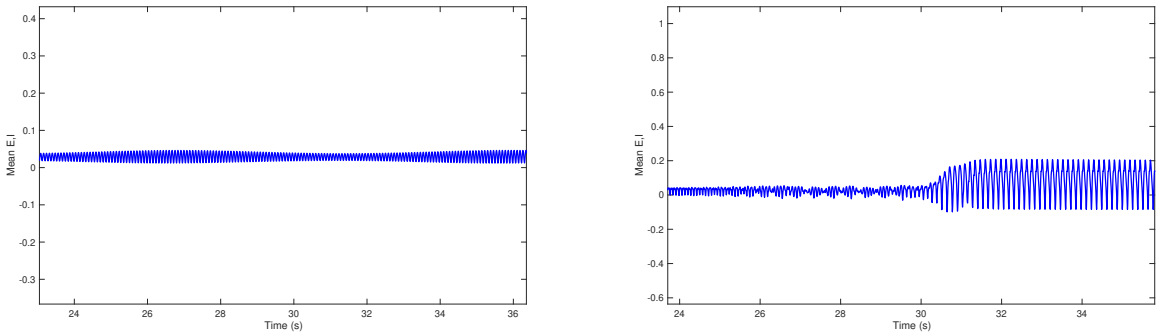

Figure 5.2: Hopf-bifurcation point beginning at $k_6 = 4$ and increasing to $k_6 = 5$ with $t = 24 - 36$s. A comparison of one unit model (left) to two-unit coupling model (right) displaying a shift in slight bursting in the single compartment model versus inceasing bursting changing into bursting spikes followed by tonic spiking in the coupling model. The change in $k_6 = 4$ shows that the Hopf-Bifurcation has been shifted back or delayed.

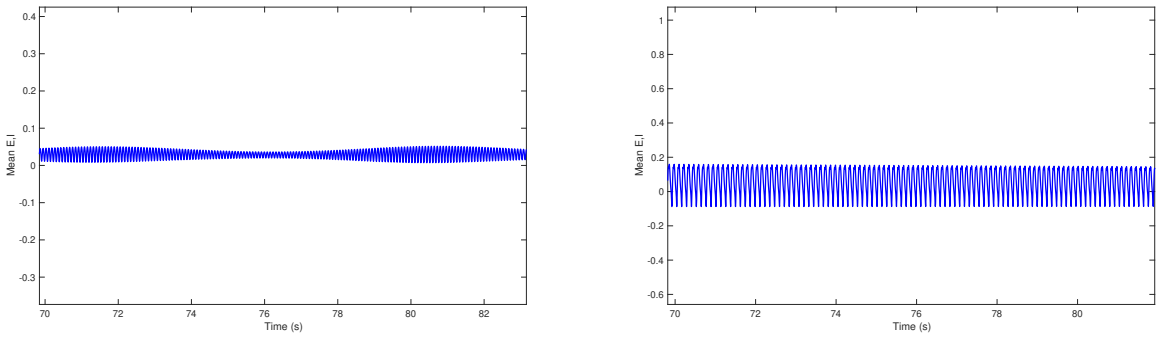

Figure 5.3: Hopf-bifurcation point beginning at $k_6 = 4$ and increasing to $k_6 = 5$ with $t = 70 - 84$s. A comparison of one unit model (left) to two-unit coupling model (right) displaying slight bursting in the single compartment model versus initial bursting followed by tonic spiking in the coupling model. An effect of coupling seen over time.

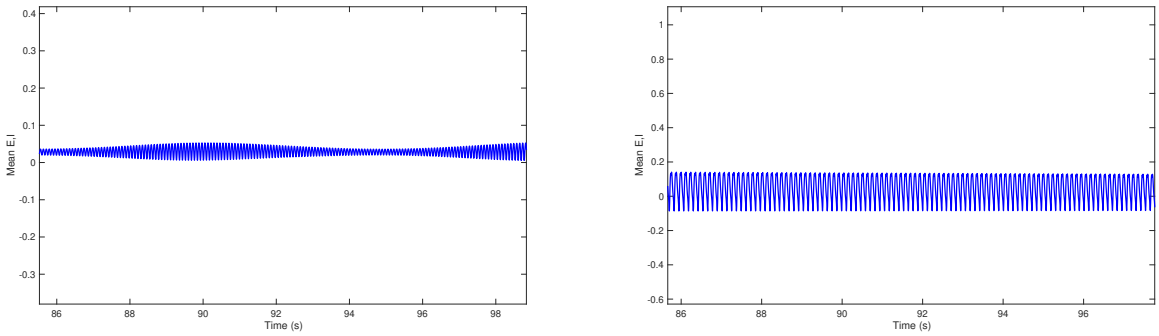

Figure 5.4: Hopf-bifurcation point beginning at $k_6 = 4$ and increasing to $k_6 = 5$ with $t = 86 - 92$s. A comparison of one unit model (left) to two-unit coupling model (right) displaying slight bursting in the single compartment model versus tonic spiking in the coupling model. Increasing coupling strength affects the spiking behavior over the entire time span.

It is evident that as k_6 increases, the thalamo-cortical oscillations are delayed. Indicative of delayed instability at time $t = 60s$ then at point $t = 69s$ Hopf-bifurcation occurs, evident by the large amplitude oscillatory behavior.

5.4 Summary of Results

In thalamic sleep rhythms and other neuronal systems in the brain [9-11,21,29,34,47-48,62], neurons have been observed experimentally to engage in a rhythmic pattern of behavior referred to as bursting. In bursting, neuronal activity alternates between active phases, characterized by large amplitude oscillations, and quiescent phases, associated with oscillations of much smaller amplitudes (see Figures 3.5-3.12 above). In this case, an absence seizure which also stems from the thalamus augments the burst a bit by adding noise to the onset of a burst causing small and large oscillatory behavior.

Mathematically, the complications involved in busting are related to a dynamical phenomenon known as delayed bifurcation or delay of stability loss, defined by Arnold [2]. Very similar activity is seen regarding the G1D model. Solutions are different at each time step. In figure 4.1-4.4, we see Thalamo-Cortical oscillations whereas no spike in the coupled unit model. Whereas, as k_6 grows larger, the coupled unit model exhibits very large oscilatory behavior and the single-unit model continues with periodic fast and low-threshold spiking. The averages between the inhibitory and excitatory populations tend to stay close to a steady state as time increases, then spiking begins at $t = 59s$. Subsequently, after a substantial time delay, solutions jump away from steady state.

CHAPTER 6

Full System Dynamics and Degree of Synchrony

6.1 Mathematical Model for Full 31-Node Network

The full network:

$$\frac{dPY_j}{dt} = (h_p - PY_j + \kappa_1 sig(PY_j) - \kappa_2 sig(IN_j) + \kappa_3 sig(TRN_j))\tau_1 + \lambda_1 \Sigma_{i,j} A(i,j)(SRN_i + \alpha_2 TRN_i)$$
$$\frac{dIN_j}{dt} = (h_i - IN_j + \kappa_4 sig(PY_j))\tau_2$$
$$\frac{dSRN_j}{dt} = (h_t - SRN_j + \kappa_5 sig(PY_j) - \frac{\kappa_6}{2}(sTRN_i))\tau_3 + \lambda_2 \Sigma_{i,j} A(i,j)(PY_i + IN_i)$$
$$\frac{dTRN_j}{dt} = (h_r - TRN_j + \kappa_7 sig(PY_j) + \frac{\kappa_8}{2}(sSRN_j) - \frac{\kappa_9}{2}(sTRN_j))\tau_4$$

6.2 Simulations

The large network consists of 31 units with 4 neuronal populations each with coupled terms to connect the total 124 equations. In order to analyze a system of this size, we used MATLAB function ODE45 to solve the system of ordinary differential equations and Mathematica NDSolve function to detect changes in nueronal activity. With MATLAB, the behavior is simulated within two minutes for 100 seconds of a neuronal process.Through many simulations and parameter sensitivity analysis, we have substantiated the fact that k_6 is the altering parameter as seen in the Taylor model. There is consistency or dormant periods followed by small oscillatory spikes in many of the simulations.

We then show activity before and after the Hopf bifurcation point in order to highlight the major differences in behavior. A comparison from non-seizure data to seizure data is shown below.

6.2.1 Varying Coupling Strength

In this section, we study how the neuronal spiking behavior changes as a result of parameter k_6. This particular parameter represents the relationship betwen Thalamic Reticular Nuclei and Specific Relay Nuclei, both populations of neurons located in the thalamus. Our goal is to not only find exact parameter values which drive these changes seen when adjusting the coupling strength but also to identify the induced transitions. The value of the k_6 parameter is augmented at each time step, $k_6 = k_6 i + \epsilon t$ in order to highlight the varying spiking behavior that could occur. Secondly, changing the strength of the coupling coefficient over the duration of the simulation in addition to the varying coupling strength. In this section, we investigate the specific range of parameter values that lead to transitions of one phase to other firing rates that may be induced from inhibitory synaptic coupling strength from TRN onto SRN.

For reference,

Parameter	Origin	Target Area	Value
κ_1	PY	PY	1.8
κ_2	IN	PY	1.5
κ_3	SRN	PY	1
κ_4	PY	IN	4
κ_5	PY	SRN	3
κ_6	TRN	SRN	varying
κ_7	PY	TRN	3
κ_8	SRN	TRN	10.5
κ_9	TRN	TRN	0.2

Table 6.1: Table of Parameter Origins and Values. Reference from Chapter 3.

$$\frac{dPY_j}{dt} = (h_p - PY_j + \kappa_1 sig(PY_j) - \kappa_2 sig(IN_j) + \kappa_3 sig(TRN_j))\tau_1 + \lambda_1 \Sigma_{i,j} A(i,j)(SRN_i + \alpha_2 TRN_i)$$
$$\frac{dIN_j}{dt} = (h_i - IN_j + \kappa_4 sig(PY_j))\tau_2$$
$$\frac{dSRN_j}{dt} = (h_t - SRN_j + \kappa_5 sig(PY_j) - \frac{\kappa_6}{2}(sTRN_j))\tau_3 + \lambda_2 \Sigma_{i,j} A(i,j)(PY_i + IN_i)$$
$$\frac{dTRN_j}{dt} = (h_r - TRN_j + \kappa_7 sig(PY_j) + \frac{\kappa_8}{2}(sSRN_j) - \frac{\kappa_9}{2}(sTRN_j))\tau_4$$

Symbol	Coupling Coefficient Initial Value	Coupling Coefficient Final Value	Increment Size
λ_1	0.2	1.2	0.01
λ_2	0.005	0.105	0.001

Table 6.2: Coupling Coefficient values for the full 31-network system

6.3 Numerical Results

In figures 5.1-5.3, we depict the average value of $(PY_j + IN_j)/2$, where $j = 1, ..., 31$ when λ_1, λ_2 are increases slowly according to the time t and $k_6 = 4$ is below the Hopf-bifurcation point. We observe as the coupling strength λ_1, λ_2 increase, the behavior of PY_j, IN_j reduces their oscillation frequence and converges to steady states.

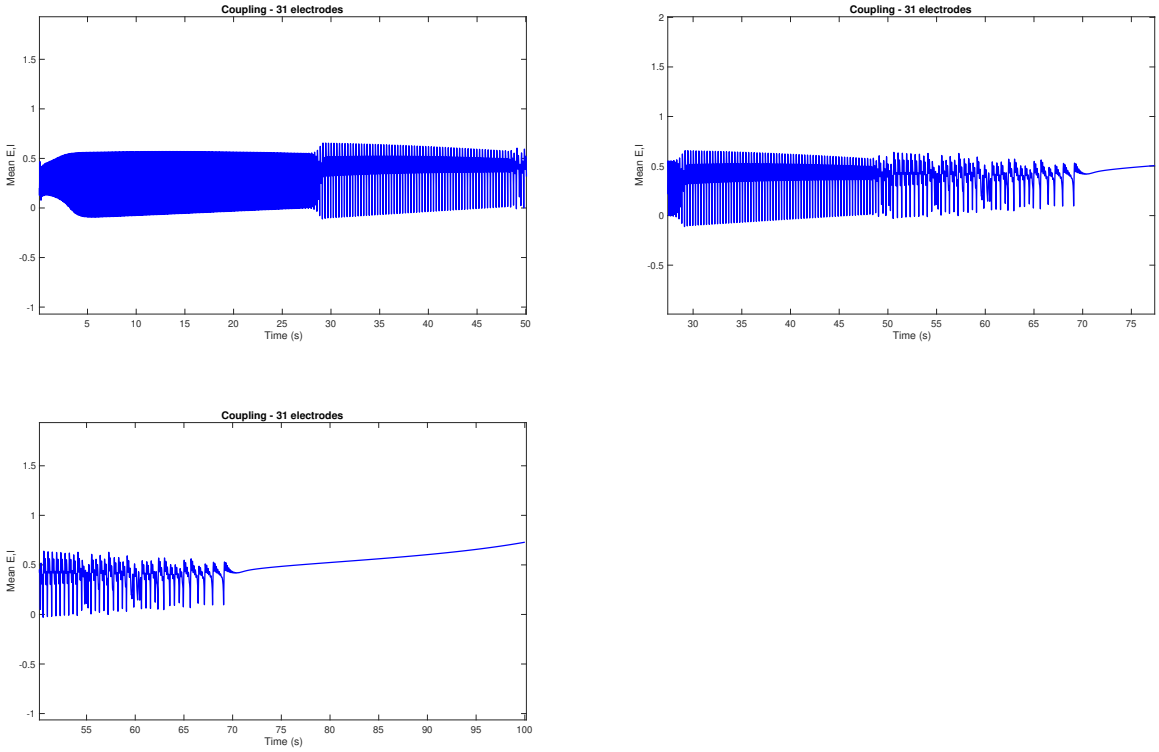

Figure 6.1: Fixed Coupling strength terms λ_1, λ_2 at 0.2 and 0.005 respectively. Spiking activity changes as Hopf-Birfurcation parameter increases from $k_6 = 4$ over time. Changes viewed as the coupling is hightened between the cortex and thalamus neuronal populations. Spiking behavior interchanges bewteen tonic, tonic bursts, spikes and lastly no activity.

6.3.1 Adding Periodic Perturbation

We then studied the changes seen when adding periodic perturbation while keeping the coupling coefficient at a fixed value then varying the coupling coefficient along with the periodic perturbation as seen in section 5, based from adaptive resonance theory for brain processing information.

$$\frac{dPY_j}{dt} = (h_p - PY_j + \kappa_1 sig(PY_j) - \kappa_2 sig(IN_j) + \kappa_3 sig(TC_j))\tau_1 \tag{6.1}$$

$$+ \lambda_1 \Sigma_{i,j} A(i,j)(SRN_i + \alpha_2 TRN_i) + \epsilon sin(\frac{\pi t}{freq}) \tag{6.2}$$

$$\frac{dIN_j}{dt} = (h_i - IN_j + \kappa_4 sig_{py})\tau_2 \tag{6.3}$$

$$\frac{dSRN_j}{dt} = (h_t - SRN_j + \kappa_5 sig(PY_j) - \frac{\kappa_6}{2}(sTRN_i))\tau_3 + \lambda_2 \Sigma_{i,j} A(i,j)(PY_i + IN_i) + \epsilon sin(\frac{\pi t}{freq}) \tag{6.4}$$

$$\frac{dTRN_j}{dt} = (h_r - TRN_j + \kappa_7 sig(PY_j) + \frac{\kappa_8}{2}(sSRN_i) - \frac{\kappa_9}{2}(sTRN_i))\tau_4 \tag{6.5}$$

6.3.2 Results

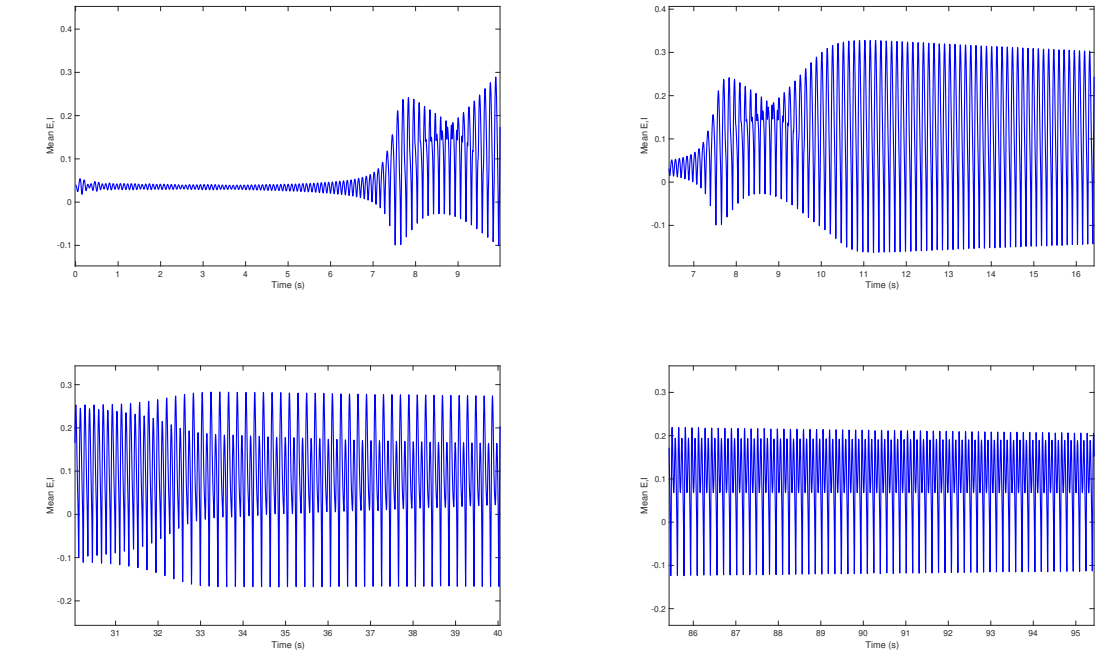

Figure 6.2: $\lambda_1 = 0.2$ and $\lambda_2 = 0.005$ with periodic perturbation increasing over time in the form of rising frequency term. Hopf-bifurcation parameter is fixed at $k_6 = 4$. The frequency term changes with ongoing frequency of the model, increasing from 31.7 Hz to 62 Hz. In addition to shifting from tonic spiking behavior. to elliptic bursting

Periodic perturbation noise stems from resonance theory. In chemistry, resonance is defined by a molecule bouncing between various valence bond structures. Within neuronal networks, the simulation of resonance is the spiking behavior altering from steady state to small oscillations, large oscillations, bursting, and tonic behavior. In Figure 6.4 we see little to no activity for the first 30 seconds then a sudden change occurs just before time $t = 48$. Solving equations 6.1-6.4 shows the solution exhibiting continuous tonic behavior.

6.3.3 Adding Noise

Secondly, we observed the changes to the system as white Gaussian noise was added. The coupling coefficients were held constant, fixed at $\lambda_1 = 0.2$ and $\lambda_2 = 0.005$, as seen in Table 6.2, in order to view the spiking changes or lack thereof without varying the coupling strengths.

$$\frac{dPY_j}{dt} = (h_p - PY_j + \kappa_1 sig(PY_j) - \kappa_2 sig(IN_j) + \kappa_3 sig(TC_j))\tau_1 \tag{6.6}$$

$$+ \lambda_1 \Sigma A(i,j)(SRN_i + \alpha_2 TRN_i) + awgn(t) \tag{6.7}$$

$$\frac{dIN_j}{dt} = (h_i - IN_j + \kappa_4 sig(PY_j))\tau_2 \tag{6.8}$$

$$\frac{dSRN_j}{dt} = (h_t - SRN_j + \kappa_5 sig(PY_j) - \frac{\kappa_6}{2}(sTRN_i))\tau_3 + \lambda_2 \Sigma A(i,j)(PY_i + IN_i) + awgn(t) \tag{6.9}$$

$$\frac{dTRN_j}{dt} = (h_r - TRN_j + \kappa_7 sig(PY_j) + \frac{\kappa_8}{2}(sSRN_i) - \frac{\kappa_9}{2}(sTRN_i))\tau_4 \tag{6.10}$$

When noise is added, numerical computations [3, 65] and asymptotic methods [28-29] suggest that the amount of delay is significantly reduced. When noise is introduced into a bursting system [29], depending on the amplitude of the noise, it

was found that there are regular patterns of alternations between a long active phase and a long silent phase, regular patterns of alternations between short active and silent phases, as well as irregular patterns of alternations of phases with various time durations. When the noise amplitude is set to be extremely close to zero, the irregular patterns give way to a pattern that strongly resembles deterministic bursting. But even with a noise of quite small magnitude, the irregularity is significant. Kuske and Baer [28-29] determine that this irregularity follows from random variation in the delay of stability loss, based on an asymptotic approximation of the probability density function for the state of the system in the silent phase and an asymptotic analysis of the effect of noise on transitions out of the active phase.

6.4 Frequency Analysis

We assume from the numerical solutions shown in previous chapters that there is a more effective way to show how well the neuronal populations synchronize. Dijkstra and Heiberg [42,43] both pose the idea of the importance of accurate models that show an appropriate response from the stimulus as seen in spiking neurons listed in chapter 1. This implies a drive response mechanism which is a result of synchronized brain activity commonly seen during an epileptic seizure [6,8]. Given that we are continually processing signals from EEG data, we must communicate vital information such as frequency, phase synchrony, general degree of synchrony and instantaneous amplitude, frequency relation to gain insight of seizure mechanism. The first section show explicitly how we evaluate frequency analysis and later define phase synchrony and degree of synchrony.

The interest of frequency analysis of EEG data has become increasingly popular, as a result various methods have been developed to evaluate amplitude and phase assessments in comparison to the various Fourier Transforms. Frequency domains

have assumptions regarding tasks and physical state of the matter involved. Various oscillations can be visualized when considering different parts of the brain. A particular task can be viewed in change in frequency.

For the full network without any changes to the model, we evaluated the frequency by counting the number of spikes over a fixed duration of time as a control. The resulting frequency was used in simulations regarding periodic perturbation.

This process was repeated for the 31-unit model with noise, increasing coupling strength, and a combination of both noise and coupling strength. Our main focus is before and during the suspected point of bifurction.

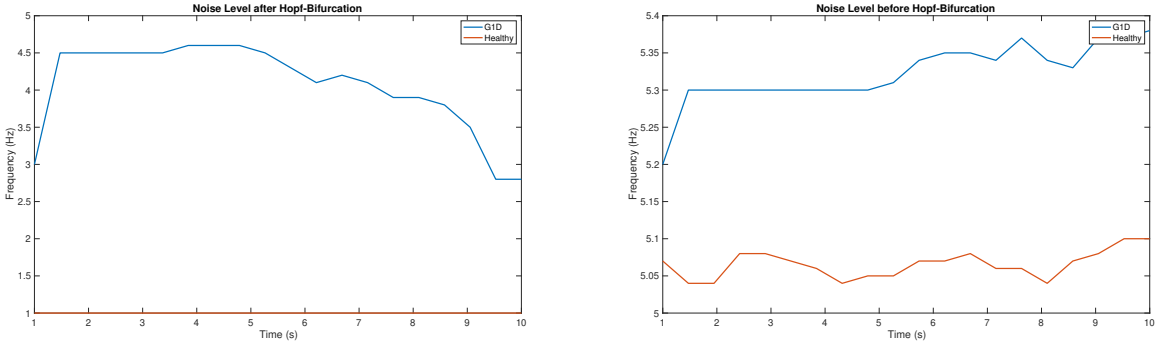

Figure 6.3: Resulting frequency of full 31-unit network model for increasing noise levels, before and after Hopf-Bifurcation. The Hopf-Bifurcation is a result of k_6 increasing from 3.5 to 4.5. A comparison between the model based from healthy (left) and then G1D (right) data.

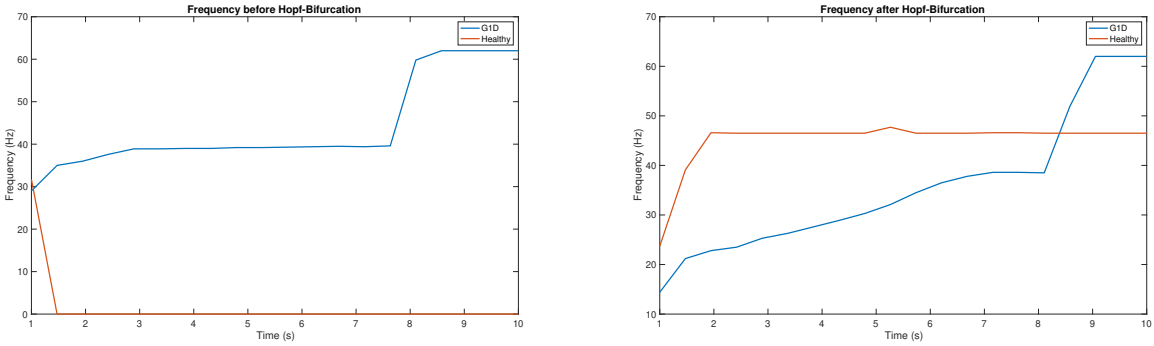

Figure 6.4: Resulting frequency of full 31-unit network model for increasing coupling strength as in Table 6.2, before and after Hopf-Bifurcation. The Hopf-Bifurcation is a result of k_6 increasing from 3.5 to 4.5. A comparison between the model based from healthy (left) and then G1D (right) data.

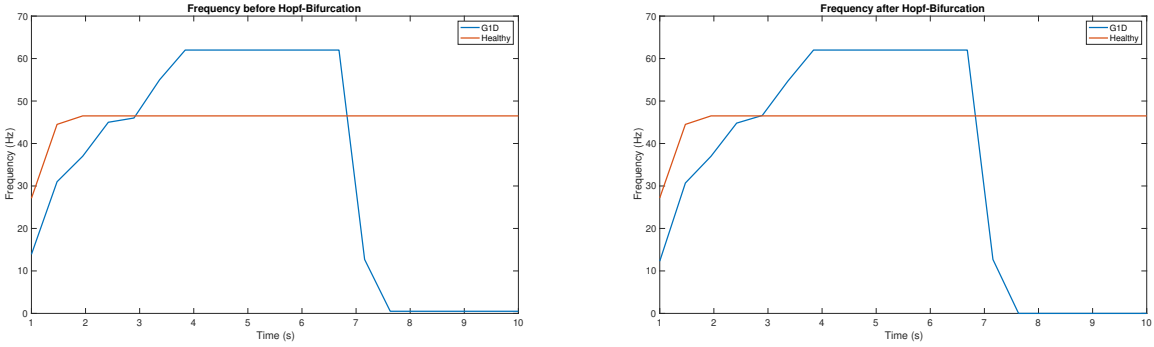

Figure 6.5: Resulting frequency of full 31-unit network model for increasing coupling strength as in Table 6.2, in addition to rising noise levels before and after Hopf-Bifurcation. The Hopf-Bifurcation is a result of k_6 increasing from 3.5 to 4.5. A comparison between the model based from healthy (left) and then G1D (right) data.

6.5 Phase Synchrony vs. Degree of Synchrony

Phase Synchrony is process commonly used due to its adaptability to time resolution. It is a three-step technique used to give further neurophysiological

information aside from frequency analysis about a patients brain rhythms. The overarching goal is to interrelate the results to cognitive processes, neurological connections, attentiveness, and much more.

The three-step process:

(1) Hilbert Transform:

$$H[x_1(t)] = \frac{1}{\pi}\text{P.V.} \int_{-\infty}^{\infty} \frac{x_1(\tau)}{t-\tau} d\tau$$

Where P.V. is the Cauchy Principal Value, a method used to assign a value to divergent integrals with odd or even integrands (or neither) and nonsymmetric intervals, under the assumption that the limit converges at the same rate.

(2) Instantaneous Phase

$$\phi_1(t) = \arctan \frac{H[x_1(t)]}{x_1(t)}$$

(3) Mean Phase Coherence

$$\text{Computed in the complex plane } \lambda = \frac{1}{N}|\Sigma_{t=1}^{N} e^{j[\phi_1(t)-\phi_2(t)]}|$$

An averaging over the membrane potential, V between two electode (signals) at time t, measuring the oscillatory populations disposition to develop total synchrony [48].

A common practive in analyzing neurologically based models is to find the value of the level of synchrony of a network of neurons or a comprehensive grouping of neurons within a network, a neuronal synchrony measure. The value of neuronal synchrony lies between 0 and 1. To truly understand the level of synchrony, one must define synchrony in terms of neurons. A group of neruons are in synch when all neurons fire action potential simultaneously, gaining a level of synchrony of 1. Conversely, 0 corresponds to asynchronization of action potentials.

Degree of synchrony is a very similar term in that pertains to a large grouping of neurons or network but incorporates the signalling process. Locally found by evaluating two signals based on the direction of their trajectory at time t. Some

researchers use a geometrical approach to evaluate the angular trajectory using cosine and sine waves while others define a measure $\chi(x, N)$ to calculate spatially decaying relationships between electrodes. In our case, due to the narrow yet long data matrix, using the method of comparing singular values was most suitable.

We did so by completing the following steps with the use of MATLAB:

- Average all four neuronal populations from the 31-unit network, then the separate excitatory and inhibitory populations, for a full 10 seconds.
- Find the singular value matrix, left singular matrix, and right singular matrix
- For each ms, the top 2 singular values we placed into a general singular value matrix, resulting in 200 singular values along the diagonal of the S matrix
- Evaluate a ratio of the singular values from the 31 electrodes for every ms

Explicit ratio formula for degree of synchrony (DOS) is:

$$DOS = (M/(M-1))(L(31)/sum(L(1) - 1/M) \tag{6.11}$$

where M is the number of electrodes and L is the list of singular values found along the diagonal of matrix S.The resulting value lies between 0 and 1, with 1 representing fully synchronized versus 0 meaning no synchrony between the channels in question.[1] We have found that multiple pathways of connection lead to various phases of synchronizations between the network of neurons, including the degree of synchronization with specific parameters.

6.5.1 Degree of Synchrony with Increased Coupling Strength

In this section, we will compare seizure data to nonseizure data within the same model in order to show the gradual differences in spiking neuronal behavior. Over

[1]Full MATLAB code is available upon request.

time we have kept the κ_i parameters constant and allowed the value of λ_i for $i = 1, 2$ to increase as seen in Table 4.1.

First, we computed a comparison of the 2-unit model with seizure and nonseizure data as the control. Then we used the same code to produce a comparison of the 31-unit model with seizure and nonseizure data.

Over time, we observed the 2-unit model to have grave impact from the increased coupling strength of $\lambda_{1,2}$ on the degree of synchrony of the system. As coupling strength increases, we see that the dregree of synchrony also increased. Considering, the 2-unit model has only 2 electrodes involved, the average excitatory and inhibitory action is much less compuationally expensive to evaluate. In additon to the fact that naturally the mean activity will never be as robust as a larger network.

In conclusion, we found that our model has much more synchronization regarding seizure data. Mathematically, larger models assume more averaging of the neuronal populations involved. In order to view the increased synchrony, we consider the degree of synchrony between arbitrary samples of the 31 units.

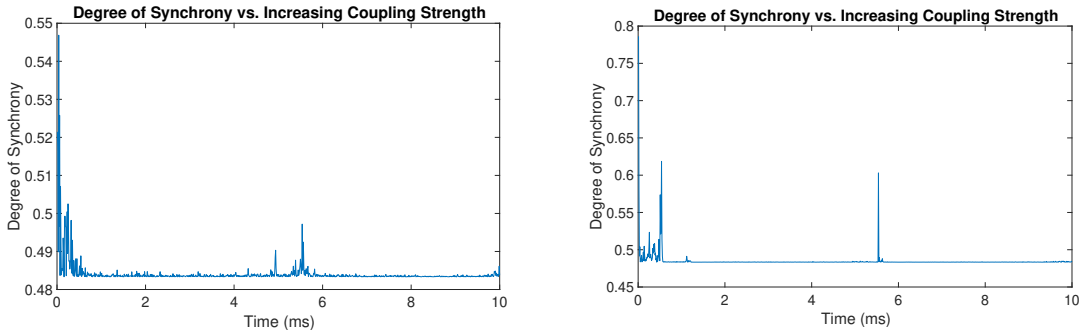

Figure 6.6: Degree of Synchrony within the 2-unit model with coupling based on non-seizure and seizure data as a result of increased coupling strength.

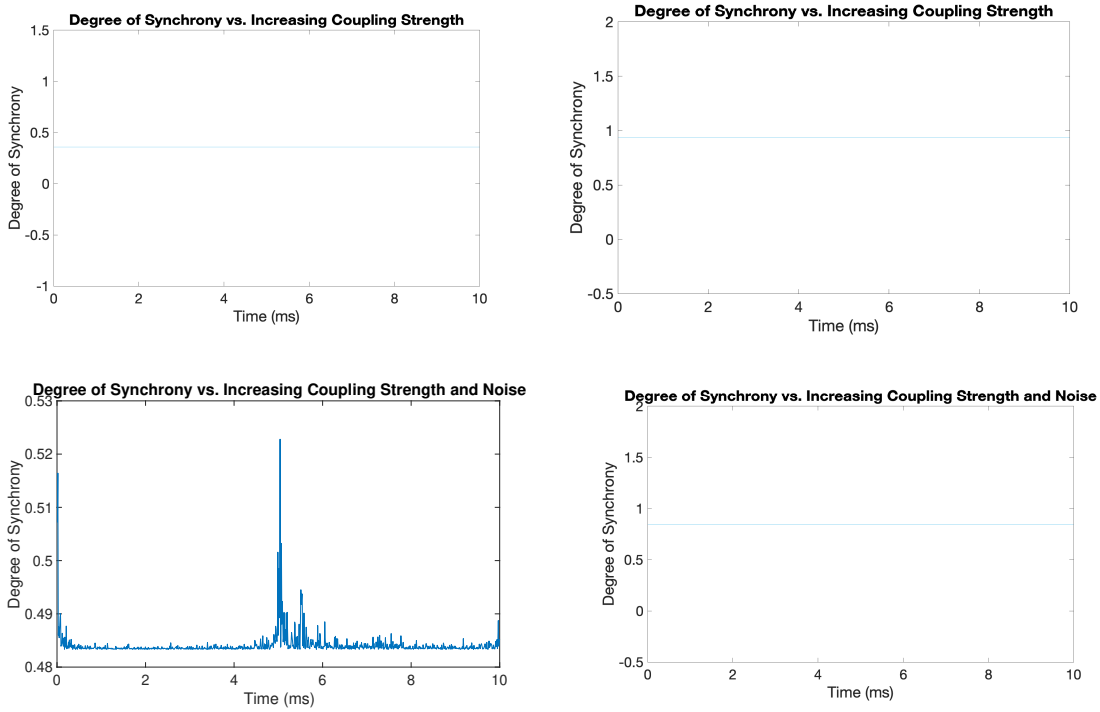

Figure 6.7: Degree of Synchrony from a sampling of 10 electrodes within the 31-unit model with coupling based on non-seizure and seizure data as a result of increased coupling strength followed by increasing coupling strength and noise level.

6.5.2 Degree of Synchrony with Increased Periodic Perturbation

Considering the full 31-unit model, we alter the periodic perturbation term and visualize the resulting degree of synchrony. The noise term is based from a periodic perturbation or resonance phenomena based theory. To do so, we calculated frequency with increasing time. Based from parameter interval for κ_6 value, $4 < \kappa_6 < 5$. As seen below, the increased noise in addition to augmented k_6 value, the degree of synchrony goes through a phase of toggling between very gradual incline and relatively steep decline then an abrupt increase that continues until the end of the time stamp. In some cases, a sudden decrease occurs as $t > 0.85$, indicates the end of seizure recording.

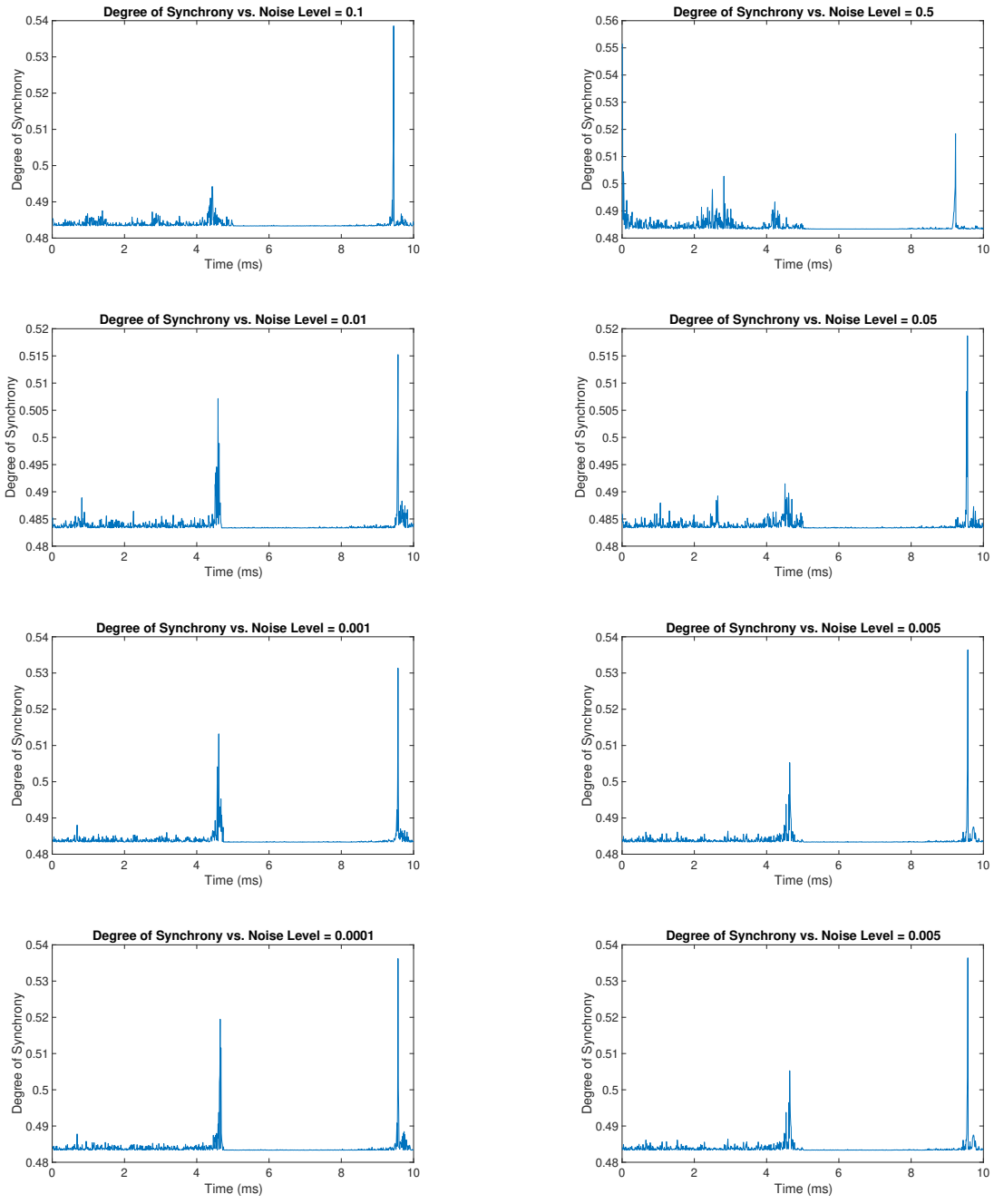

Figure 6.8: Degree of Synchrony within the 31-unit model with coupling based on seizure data with level of periodic perturbation set at (a) 0.1 (b) 0.5 (c) 0.01 (d) 0.05 (e) 0.001 (f) 0.005 (g) 0.0001 (h) 0.0005.

6.5.3 Degree of Synchrony with Increased Periodic Perturbation and Coupling Strength

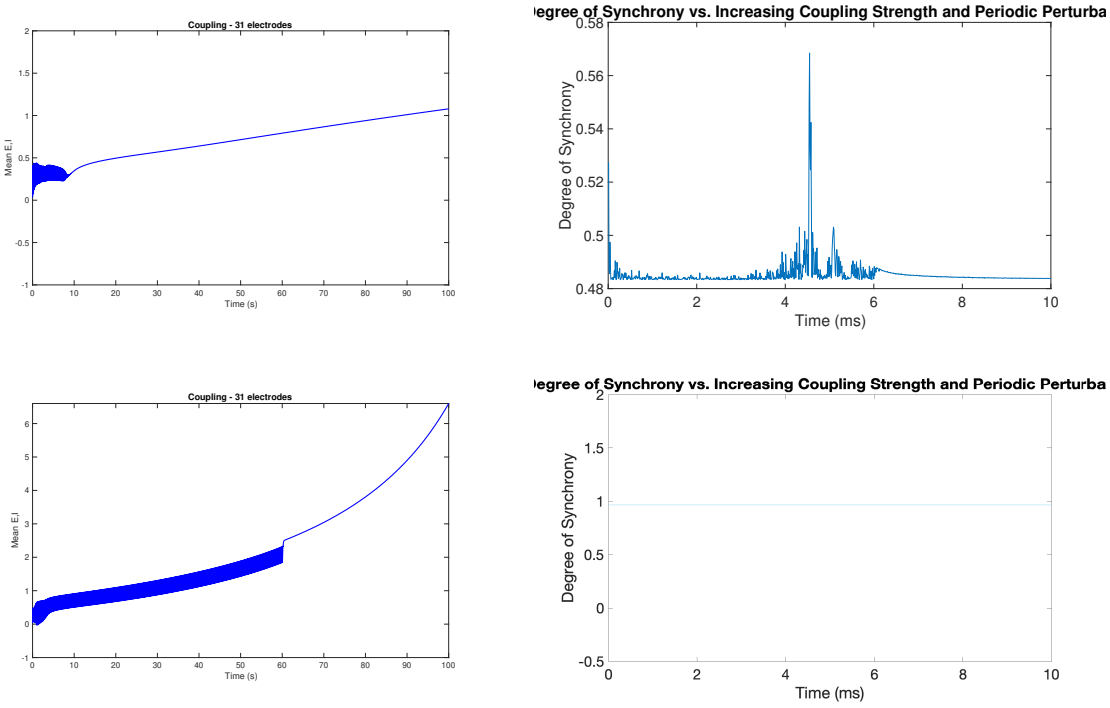

Figure 6.9: Degree of Synchrony within the 31-unit model with coupling based on non-seizure (top) and seizure (bottom) data as a result of increased coupling strength and periodic perturbation.

6.6 Summary of Results

De Vries and Sherman [7] both studied the electrical behavior of coupled pancreatic β-cells with a focus on the beneficial influence of noise. However, small random perturbations may have dramatic effects on dynamical systems and lead to the emergence of new dynamical behaviors [8]. Stochastic resonance is a well-known [9, 10] example. The term stochastic resonance is given to a phenomenon that is

manifest in nonlinear systems whereby generally feeble input information (such as a weak signal) can be amplified and optimized by the assistance of noise [9].

It was suggested previously that stochastic fluctuations of ion channels in the plasma membrane are responsible for disrupting bursting behavior and transforming isolated cells to spikers, but that the effective sharing of channels by electrically coupled cells averages the noise and lets the bursting phenomena appear [16]. This was later analyzed in [17, 18] using mathematical modeling. In [19], the work of Pedersen and Sorensen supports previous investigations of the channel sharing hypothesis by the application of two recent methods, which allow an analytic treatment of stochastic effects on the location of the saddle-node and homoclinic bifurcations that are relevant to bursting activity. The work of Su et al. [20] also analytically characterizes the influence of noise on phase switching, in the case of elliptic bursting dynamics.

Neurons show significant variation in the presence and timing of action potentials across stimulus trials, a phenomenon whose function and significance has been the subject of great interest. Cortical activity is characterized by highly irregular interspike intervals.

From our simulations, we are able to find specific parameter ranges that which cause a class or classes of diseased state spiking neuron. $t = 0 - 27$, $t = 28 - 45$, $t = 46 - 54$, and $t = 54 - 77$ all signify a change in spiking neuron characterized as tonic bursting, thalmaocortical oscillations, and spindles. One positive effect on noise and bifurcation is they have modified the synchronization of the network, both through delayed bifurcation and noise, as a result of coupling.

The setting of the mathematical results are very general, the mechanism is working for a large class of equations. However, we were able to see a comparison of preseizure and seizure network in this chapter, concluding that the seizure is highly synchronized as coupling strength increases and the addition of noise. Th

CHAPTER 7

Conclusion and Future Work

Several computational neurological models have been developed over the last 40 years for small and large neuronal networks, cellular models for ion channel dynamics, and mathematical models to visualize the effect of neuronal connections between the cortex and thalamus. In order to retrieve a full picture of patterns seen in EEG data, it has been proven in literature that a thalamocortical coupled model is best.

In chapter two, we found that our graphs do give a useful visual as to how well the brain is connected in a healthy or non seizure activity. Yet it may not give an effective or accurate analysis of how synchronized various brain regions are connected before and during a seizure. The correlation plot will only give an average at just one timepoint considered rather than a fixed time period so incorporating this information within the model was imperative. In chapter 3, we more closely studied the single compartment and two-unit coupled model. It was found that an absence seizure augments the elliptic burst a bit by adding noise to the onset of an elliptic burst. Consequently, after a substantial time delay, solutions jump away from steady state. In chapter 4, it was shown using matrix operations that coupling strength and self-interference terms impact stability of the system in addition to delaying the Hopf-bifurcation. Lastly, in chapter 5, after a comparison of preseizure and seizure network, we found that the seizure data causes the system to be highly synchronized as coupling strength increases and the addition of noise.

In this study, we produced a ODE model comprised of four neuronal populations that are most active in Glucose Transport Deficiency Type 1 Epilepsy. We

characterized spiking behavior changes seen as a result of varying coupling strength and noise. Overall, our research has given a better picture of the dynamical properties seen from this form of epilepsy. This model described the spiking neuronal activity seen an epileptic induced seizure network through. By dissecting the correlation association of neuronal units or electrodes, the subpopulations of the cortex and thalamus in seizure data, certain patterns were classified. Our model is versatile in the manner in which simulations can be produced with a change in coupling and the addition of coupling strengths. The model is built to highlight the connections in the network derived from data.

We plan to continue our work by closely studying sensitivity analysis regarding parameters that directly affect SWD and spindles using Partial Rank Correlation Coefficient. We would also consider neurological sensitivities with respects to the self-interference terms represented by c_i values in our model. Our large model could be more accurate with an increased data based model comparison to more G1D patients. Lastly, analyzing a visual representation of sparsity within the larger spatial inverse problem yielded from the source patterns.

APPENDIX A

Appendix

A.1 Equilibrium Relation from Single-compartment Model

A.1.1 Routh Hurwitz Criterion

$a_0 > 0$, $a_1 > 0$, $a_1a_2 - a_0a_3 > 0$, $a_1a_2a_3 - a_1^2a_4 - a_0a_3^2 > 0$, and $a_4 > 0$

- $a_0 > 0$ yields $1 > 0$
- $a_1 > 0$ yields $(c_2\tau_2 + c_3t_3 + c_1\tau_1 - \frac{\kappa_1\tau_1}{200} + c_4\tau_4 + c_4\kappa_9 s\tau_4) > 0$
- $a_1a_2 - a_0a_3 > 0$ yields $(c_2\tau_2 + c_3t_3 + c_1\tau_1 - \frac{\kappa_1\tau_1}{200} + c_4\tau_4 + c_4\kappa_9 s\tau_4)(\frac{\kappa_4\kappa_2\tau_2\tau_1}{40000} + c_1c_4\tau_1\tau_4 - \frac{c_4\kappa_1\tau_1\tau_4}{200} - \frac{\kappa_3\kappa_7\tau_1\tau_4}{40000} + c_1c_4\kappa_9 s\tau_1\tau_4 - \frac{c_4\kappa_1\kappa_9 s\tau_1\tau_4}{200} + (c_2\tau_2 + c_2\tau_3)(c_1\tau_1 - \frac{\kappa_1\tau_1}{200} + c_4\tau_4 + c_4\kappa_9 s\tau_4) + c_2c_3t_2t_3 + (\kappa_8c_3s\tau_4)(c_4\kappa_6 s\tau_3)) - ((\frac{\kappa_4\kappa_2\tau_2\tau_1}{40000})(c_3\tau_3 + c_4t_4 + \kappa_9 s c_4\tau_4) + (c_2c_3\tau_2\tau_4)(c_1\tau_1 - \frac{\kappa_1\tau_1}{200} + c_4\tau_4 + c_4\kappa_9 s\tau_4) + (\kappa_8c_3s\tau_4)(-\frac{\kappa_3\kappa_5\tau_1\tau_2}{40000} + c_1c_4\kappa_6 s\tau_1\tau_3 - \frac{c_4\kappa_1\kappa_6 s\tau_1\tau_3}{200}) + (c_2\tau_2\kappa_8c_3s\tau_4)(c_4\kappa_6 s\tau_3)) > 0$
- $a_1a_2a_3 - a_1^2a_4 - a_0a_3^2 > 0$ yields $(c_2\tau_2 + c_3t_3 + c_1\tau_1 - \frac{\kappa_1\tau_1}{200} + c_4\tau_4 + c_4\kappa_9 s\tau_4)(\frac{\kappa_4\kappa_2\tau_2\tau_1}{40000} + c_1c_4\tau_1\tau_4 - \frac{c_4\kappa_1\tau_1\tau_4}{200} - \frac{\kappa_3\kappa_7\tau_1\tau_4}{40000} + c_1c_4\kappa_9 s\tau_1\tau_4 - \frac{c_4\kappa_1\kappa_9 s\tau_1\tau_4}{200} + (c_2\tau_2 + c_2\tau_3)(c_1\tau_1 - \frac{\kappa_1\tau_1}{200} + c_4\tau_4 + c_4\kappa_9 s\tau_4) + c_2c_3t_2t_3 + (\kappa_8c_3s\tau_4)(c_4\kappa_6 s\tau_3))((\frac{\kappa_4\kappa_2\tau_2\tau_1}{40000})(c_3\tau_3 + c_4t_4 + \kappa_9 s c_4\tau_4) + (c_2c_3\tau_2\tau_4)(c_1\tau_1 - \frac{\kappa_1\tau_1}{200} + c_4\tau_4 + c_4\kappa_9 s\tau_4) + (\kappa_8c_3s\tau_4)(-\frac{\kappa_3\kappa_5\tau_1\tau_2}{40000} + c_1c_4\kappa_6 s\tau_1\tau_3 - \frac{c_4\kappa_1\kappa_6 s\tau_1\tau_3}{200}) + (c_2\tau_2\kappa_8c_3s\tau_4)(c_4\kappa_6 s\tau_3)) - ((\frac{\kappa_4\kappa_2\tau_2\tau_1}{40000})(c_3\tau_3 + c_4t_4 + \kappa_9 s c_4\tau_4) + (c_2c_3\tau_2\tau_4)(c_1\tau_1 - \frac{\kappa_1\tau_1}{200} + c_4\tau_4 + c_4\kappa_9 s\tau_4) + (\kappa_8c_3s\tau_4)(-\frac{\kappa_3\kappa_5\tau_1\tau_2}{40000} + c_1c_4\kappa_6 s\tau_1\tau_3 - \frac{c_4\kappa_1\kappa_6 s\tau_1\tau_3}{200}) + (c_2\tau_2\kappa_8c_3s\tau_4)(c_4\kappa_6 s\tau_3))^2 > 0$
- $a_4 > 0$ yields $(\frac{\kappa_2\kappa_4\tau_1\tau_2}{40000})(c_3\tau_3c_4\tau_4 + c_3\tau_3\kappa_9 s c_4\tau_4 + \kappa_8 s^2 c_3\tau_4\kappa_6 c_4\tau_3) + (c_2c_3\tau_2\tau_3)(c_1c_4\tau_1\tau_4 - \frac{c_4\kappa_1\kappa_6 s\tau_1\tau_3}{200}) + (c_2c_3\kappa_8 s\tau_2\tau_4)(-\frac{\kappa_2\kappa_4\tau_1\tau_2}{40000} + c_1c_4\kappa_6 s\tau_1\tau_3 - \frac{c_4\kappa_1\kappa_6 s\tau_1\tau_3}{200}) > 0$

A.1.2 Finding Equilibria of 1-D model, used before Cramers Rule

First, we approximate sig_{NP} by a linear approximation $\frac{NP}{200} + \frac{1}{2}$, where NP is the neuronal population. Then, we assume $PY^* \neq 0$, $\tau_1 \neq 0$, and set (4.1) equal to zero to obtain

$$0 = (h_p - c_1PY^* + \kappa_1(\frac{PY^*}{200} + \frac{1}{2}) - \kappa_2(\frac{IN^*}{200} + \frac{1}{2}) + \kappa_3(\frac{TRN^*}{200} + \frac{1}{2}))\tau_1 + a_1\lambda_1$$

$$-\frac{a_1\lambda_1}{\tau_1} = h_p - c_1 PY^* + \kappa_1(\frac{PY^*}{200} + \frac{1}{2}) - \kappa_2(\frac{IN^*}{200} + \frac{1}{2}) + \kappa_3 * (\frac{TRN^*}{200} + \frac{1}{2})$$

$$PY^*(\frac{\kappa_1 - 200c_1}{200}) = -\frac{a_1\lambda_1}{\tau_1} - \frac{(\kappa_1 + \kappa_3)}{2} + \kappa_2\frac{IN^* + 100}{200} - h_p - \frac{\kappa_3 TRN^*}{200}$$

Therefore,

$$PY^* = (\tfrac{a_1\lambda_1}{\tau_1} - \tfrac{(\kappa_1+\kappa_3)}{2} + \kappa_2\tfrac{IN^*+100}{200} - h_p - \tfrac{\kappa_3 TRN^*}{200})(\tfrac{200}{\kappa_1 - 200c_1})$$

We choose to place c_i along with the state variables because the amount of inference from neighboring populations, which we will see later in section 2, does affect stability.

Secondly, we set (4.2) equal to zero. Under the assumption, $IN^* \neq 0$ and $\tau_2 \neq= 0$,

$$(h_i - c_2 IN^* + \kappa_4(\frac{PY^*}{200} + \frac{1}{2}))\tau_2 = 0$$

$$IN^* = \frac{h_i}{c_2} - \frac{\kappa_4}{c_2}(\frac{PY^* + 100}{200})$$

Now, set (4.3) equal to zero to get

$$0 = (h_r - c_3 SRN^* + \kappa_5(\frac{PY^*}{200} + \frac{1}{2}) - \frac{\kappa_6}{2}(sTRN^*))\tau_3$$

$$SRN^* = [-\frac{0.96\lambda_1}{\tau_3} + h_r + \kappa_5(\frac{PY^* + 100}{200}) - \kappa_6(sTRN^* + \frac{1}{2})](\frac{1}{c_3})$$

Hence,

$SRN^* = [-\frac{0.96\lambda_1}{\tau_3} + h_r + \kappa_5(\frac{PY^*+100}{200}) - \kappa_6(sTRN^* + \frac{1}{2})](\frac{1}{c_3})$.

Lastly, we set (4.4) equal to zero to get

$$0 = (h_t - c_4 TRN^* + \kappa_7(\frac{PY^*}{200} + \frac{1}{2}) + \frac{\kappa_8}{2}(sSRN^*) - \frac{\kappa_9}{2}(sTRN^*))\tau_4$$

$$(-\tau_4(c_4 + \frac{s\kappa_9}{2}))TRN^* = (h_t + \kappa_7(\frac{PY^*}{200} + \frac{1}{2}) + \frac{\kappa_8}{2}(sSRN^*))\tau_4$$

Thus,

$TRN^* = (-\frac{1}{\tau_4(c_4+\frac{s\kappa_9}{2})})(h_t + \kappa_7(\frac{PY^*}{200} + \frac{1}{2}) + \frac{\kappa_8}{2}(sSRN^*))$

A.2 Proof of 4 cases in Section 4.1

Let $\lambda = uc_1 + wc_3$, where c_1 and c_3, self-interference terms for pyramidal and specific relay neurons. We then consider four cases:

1 u, w are both real and positive or negative

2 u, w are both real and either positive or negative

3 u, w are both complex with positive real parts

4 u, w are both complex with negative real parts

Then solve $detA = 0$ to find all eigenvalues.[1] Case 1: Let $u, w \in \mathbb{R}^+$ then

$$\begin{aligned}(uc_1 + wc_3 - (a+ib))^2 - \gamma^2 &= [(uc_1 + wc_3 - a) - ib]^2 - \gamma^2 \\ &= ((uc_1 + wc_3 - a)^2 - (ib)^2) + 2i((-ib)(uc_1 + wc_3 - a)) - \gamma^2 \\ &= ((uc_1 + wc_3 - a)^2 - (ib)^2) + 2((b)(uc_1 + wc_3 - a)) - \gamma^2 \\ &= (uc_1 + 2wc_3 - 2a - 2ib)uc_1 + (wc_3 - 2a - 2ib)wc_3 + a^2 - b^2 + 2ib - \gamma^2\end{aligned}$$

If $2a > uc_1 + 2wc_3$ and $2a > wc_3$ then λ is stable.

Second eigenvalue:

$$\begin{aligned}(uc_1 + wc_3 + (a+ib))^2 - \gamma^2 &= [(uc_1 + wc_3 + a) + ib]^2 - \gamma^2 \\ &= ((uc_1 + wc_3 + a)^2 + (ib)^2) + 2i((ib)(uc_1 + wc_3 + a)) - \gamma^2 \\ &= ((uc_1 + wc_3 + a)^2 - (ib)^2) + 2((b)(uc_1 + wc_3 + a)) - \gamma^2 \\ &= (uc_1 + 2wc_3 + 2a - 2ib)uc_1 + (wc_3 + 2a + 2ib)wc_3 + a^2 - b^2 + 2ib - \gamma^2\end{aligned}$$

If $uc_1 + 2wc_3 < 2a$ and $wc_3 + 2a < 0$ then λ is stable.

[1] Poof of all cases shown in Appendix A

Case 2: Let $u \in \mathbb{R}^+$ and $w \in \mathbb{R}^-$ then part (a) of Case 1 will yield

$$(uc_1+wc_3-(a+ib))^2-\gamma^2 = (uc_1+2wc_3-2a-2ib)uc_1+(wc_3-2a-2ib)wc_3+a^2-b^2+2ib-\gamma^2 \tag{A.1}$$

Implying that if $(uc_1 + 2wc_3 - 2a)uc_1 + (wc_3 - 2a)wc_3 + a^2 - b^2 < 0$ then λ is stable. Similar stability statement for $u \in \mathbb{R}^-$ and $w \in \mathbb{R}^+$.

Case 3: Let $u, w \in$ with positive real parts where $u, w \neq 0$ then

$$\begin{aligned}((uc_1 + wc_3) - (a + ib))^2 - \gamma^2 &= ((u_1c_1 + w_1c_3 - a) + i(u_2c_1 + w_2c_3 - b))^2 - \gamma^2 \\ &= (u_1c_1 + w_1c_3 - a)^2 + 2i(u_1c_1 + w_1c_3 - a)(u_2c_1 + w_2c_3 - b) \\ &\quad - (u_2c_1 + w_2c_3 - b)^2 - \gamma^2\end{aligned}$$

Case 4: Let $u, w \in$ with negative real parts where $u, w \neq 0$ then the proof is similar to that of Case 3. In both cases, the eigenvalues will be complex, stability will hold if the real part of λ is negative. ■

REFERENCES

[1] Suczynski, P., Kalitzin, S., & Da Silva, F. L. (2004). Dynamics of non-convulsive epileptic phenomena modeled by a bistable neuronal network. *Neuroscience*, 126(2),467-484.

[2] Lytton, William W., et al. "Dynamic interactions determine partial thalamic quiescence in a computer network model of spike-and-wave seizures." *Journal of Neurophysiology* 77.4 (1997): 1679-1696.

[3] Taylor, P.N., et al. (2014). A computational study of stimulus induced driven epileptic seizure abatement. *PLoS One*, 9(12), e114316.

[4] Yan, Z. (2005). A new scheme to generalized (lag, anticipated, and complete) synchronization in chaotic and hyperchaotic systems. Chaos, 15(1), 13101.

[5] Gerstner, Wulfram. "2.2 Hodgkin-Huxley Model." 2.2 Hodgkin-Huxley Model Neuronal Dynamics Online Book, 2014, neuronaldynamics.epfl.ch/online/Ch2.S2.html.

[6] Connecting thegrowing brain. "Epilepsy and the Synapse." Connecting the Growing Brain, 2018, www.connectingthegrowingbrain.com/np-diseases-and-synapsis/epilepsy-and-the-synapse/.

[7] Mastin, Luke. "NEURONS & SYNAPSES." Memory Recall/Retrieval - Memory Processes - The Human Memory, 2018, www.human-memory.net/brain_neurons.html.

[8] Baier, Gerold, et al. "The Importance of Modeling Epileptic Seizure Dynamics as Spatio-Temporal Patterns." Frontiers in Physiology, vol. 3, 17 July 2012, doi:10.3389/fphys.2012.00281.

[9] Bekkers, John M. "Pyramidal Neurons." Current Biology, vol. 21, no. 24, 20 Dec. 2011, doi:10.1016/j.cub.2011.10.037.

[10] Gonzales, R.B., DeLeon Galvan, C.J., Rangel, Y.M., and Claiborne, B.J. (2001). Distribution of thorny excrescences on CA3 pyramidal neurons in the rat hippocampus. J. Comp. Neurol. 430,357–368.

[11] Nelson, S.B., Hempel, C., and Sugino, K. (2006). Probing the transcriptome of neuronal cellmtypes. Curr. Opin. Neurobiol. 16, 571–576.

[12] Spruston, Nelson. "Pyramidal Neurons: Dendritic Structure and Synaptic Integration." Nature Reviews Neuroscience, vol. 9, no. 3, Mar. 2008, pp. 206–221., doi:10.1038/nrn2286.

[13] Markram H., Maria Toledo-Rodriguez, Yun Wang, Anirudh Gupta, Gilad Silberberg & Caizhi Wu (2004). Interneurons of the neocortical inhibitory system, Nature Reviews Neuroscience, 5 (10) 793-807. DOI: http://dx.doi.org/10.1038/nrn1519

[14] Rudy B. & Chris J. McBain (2001). Kv3 channels: voltage-gated K channels designed for high-frequency repetitive firing, Trends in Neurosciences, 24 (9) 517-526. DOI: http://dx.doi.org/10.1016/s0166-2236(00)01892-0

[15] Ma W.P., B.-h. Liu, Y.-t. Li, Z. Josh Huang, L. I. Zhang & H. W. Tao (2010). Visual Representations by Cortical Somatostatin Inhibitory Neurons–Selective But with Weak and Delayed Responses, Journal of Neuroscience, 30 (43) 14371-14379. DOI:http://dx.doi.org/10.1523/jneurosci.3248-10.2010

[16] "Chapter III - The Afferent Axons to the Thalamus." Exploring the Thalamus, by S. Murray. Sherman and R. W. Guillery, Academic Press, 2001, pp. 59–108.

[17] Pinault, Didier. "The Thalamic Reticular Nucleus: Structure, Function and Concept." Brain Research Reviews, vol. 46, no. 1, Aug. 2004, pp. 1–31., doi:10.1016/j.brainresrev.2004.04.008.

[18] Williams, John. "What Is the Limbic System in the Brain?" What Is the Limbic System in the Brain? - Definition, Functions Parts Video,

Study.com, 2018, study.com/academy/lesson/what-is-the-limbic-system-in-the-brain-definition-functions-parts.html.

[19] "NORD (National Organization for Rare Disorders)." Glucose Transporter Type 1 Deficiency Syndrome, 2017, rarediseases.org/rare-diseases/glucose-transporter-type-1-deficiency-syndrome/.

[20] Taylor, P. N., & Baier, G. (2011). A spatially extended model for macroscopic spike-wave discharges. Journal of computational neuroscience, 31(3), 679-684.

[21] Taylor, P. N., Baier, G., Cash, S. S., Dauwels, J., Slotine, J. J., & Wang, Y. (2013). A model of stimulus induced epileptic spike-wave discharges. IEEE Symposium on Computational Intelligence, Cognitive Algorithms, Mind, and Brain (CCMB),9(5), 53-59.

[22] Taylor, P. N., Thomas, J., Sinha, N., Dauwels, J., Kaiser, M., Thesen, T., & Ruths, J. (2015). Optimal control based seizure abatement using patient derived connectivity. Frontiers in neuroscience,1(9), 202.

[23] Taylor, P. N., Wang, Y., Goodfellow, M., Dauwels, J., Moeller, F., Stephani, U., et al. (2014). A computational study of stimulus driven epileptic seizure abatement. PloS one, 9(12), e114316.

[24] Traub, R. D., Contreras, D., Cunningham, M. O., Murray, H., Lebeau, F. E. N., Roopun, A., et al. (2005). Single-column thalamocortical network model exhibiting gamma oscillations, sleep spindles, and epileptogenic bursts. Journal of Neurophysiology

[25] Swenson, Rand. "Chapter 10 - Thalamic Organization." Chapter 10: The Thalamus, 2006, www.dartmouth.edu/ rswenson/NeuroSci/chapter_10.html.

[26] Reyes, Sam. "Auditory Divisions of Thalamus." Auditory System: Anatomic Tour, Library of Congress Web Archives, 2001, webarchive.loc.gov/all/20011127072157/http://serous.med.buffalo.edu/hearing/thalamus.html.

[27] Crosson, B. A. (1992). Subcortical functions in language and memory. New York, NY, US: Guilford Press.

[28] FITZGERALD, M J Turlough (2012). Clinical Neuroanatomy and Neuroscience. Philadelphia: Saunders Elsevier. pp. 284–285. ISBN 978-0-7020-3738-2.

[29] SWENSON, Rand. "Chapter 10 - Thalamic Organization". Review of clinical and functional neuroscience. Dartmouth Medical School. Retrieved 9 May 2012.

[30] Ermentrout B. (1998) Neural networks as spatio-temporal pattern-forming systems. Rep Prog Phys 61(4):353

[31] Ermentrout GB, Cowan JD (1979) A mathematical theory of visual hallucination patterns. Biol Cybern 34(3):137–150

[32] Kilpatrick, Zachary P. "Wilson-Cowan Model." Encyclopedia of Computational Neuroscience, 2013, pp. 1–5., doi:10.1007/978-1-4614-7320-6_80-1.

[33] Wilson HR, Cowan JD (1972) Excitatory and inhibitory interactions in localized populations of model neurons. Biophys J 12(1):1–24

[34] Wilson HR, Cowan JD (1973) A mathematical theory of the functional dynamics of cortical and thalamic nervous tissue. Kybernetik 13(2):55–80

[35] Taylor, Peter Neal, and Gerold Baier. "A Spatially Extended Model for Macroscopic Spike-Wave Discharges." Journal of Computational Neuroscience, vol. 31, no. 3, 2011, pp. 679–684., doi:10.1007/s10827-011-0332-1.

[36] Taylor, Peter N, et al. "Epileptic Spike-Wave Discharges in a Spatially Extended Thalamocortical Model." BMC Neuroscience, vol. 14, no. S1, 2013, doi:10.1186/1471-2202-14-s1-p87.

[37] Fan, Denggui, et al. "Stimulus-Induced Epileptic Spike-Wave Discharges in Thalamocortical Model with Disinhibition." Scientific Reports, vol. 6, no. 1, 2016, doi:10.1038/srep37703.

[38] Taylor, Peter N., et al. "A Model of Stimulus Induced Epileptic Spike-Wave Discharges." 2013 IEEE Symposium on Computational Intelligence, Cognitive Algorithms, Mind, and Brain (CCMB), 2013, doi:10.1109/ccmb.2013.6609165.

[39] Fan, Denggui, et al. "Rich Dynamics Induced by Synchronization Varieties in the Coupled Thalamocortical Circuitry Model". *Brain Informatics: International Conference, BI 2018*. Springer, vol. 11309, 2018, pp. 78–84.

[40] Kumarahirwal, Mitul, and Narendra D Londhe. "Power Spectrum Analysis of EEG Signals for Estimating Visual Attention." *International Journal of Computer Applications*, vol. 42, no. 15, 2012, pp. 34–40., doi:10.5120/5769-7993.

[41] Izhikevich, E.m. "Simple Model of Spiking Neurons." *IEEE Transactions on Neural Networks*, vol. 14, no. 6, Nov. 2003, pp. 1569–1572., doi:10.1109/tnn.2003.820440.

[42] Heiberg, Thomas, et al. "Firing-Rate Models for Neurons with a Broad Repertoire of Spiking Behaviors." *BMC Neuroscience*, vol. 14, no. S1, 27 Aug. 2018, doi:10.1186/1471-2202-14-s1-p317.

[43] Dijkstra, Koen, et al. "A Rate-Reduced Neuron Model for Complex Spiking Behavior." *The Journal of Mathematical Neuroscience*, vol. 7, no. 1, 11 Dec. 2017, doi:10.1186/s13408-017-0055-3.

[44] Fan, Denggui, et al. "Stimulus-Induced Transitions between Spike-Wave Discharges and Spindles with the Modulation of Thalamic Reticular Nucleus." *Journal of Computational Neuroscience*, vol. 43, no. 3, 2017, pp. 203–225., doi:10.1007/s10827-017-0658-4.

[45] Bhattacharyya, Sourya, et al. "Automatic Sleep Spindle Detection in Raw EEG Signal of Newborn Babies." *2011 3rd International Conference on Electronics Computer Technology*, 7 July 2011, doi:10.1109/icectech.2011.5941563.

[46] Asla Pitkänen et al."Pharmacologically Induced Animal Models of Absence Seizures." Models of Seizures and Epilepsy, *Academic Press*, 2017, pp. 553–562.

[47] Golomb, David. "Neuronal Synchrony Measures." Scholarpedia, *Brain Corporation*, 2007, www.scholarpedia.org/article/Neuronal_synchrony_measures.

[48] Kopell, N., et al. "Gamma Rhythms and Beta Rhythms Have Different Synchronization Properties." *Proceedings of the National Academy of Sciences*, vol. 97, no. 4, 2000, pp. 1867–1872., doi:10.1073/pnas.97.4.1867.

[49] Traub, R. D., et al. "A Model of a CA3 Hippocampal Pyramidal Neuron Incorporating Voltage-Clamp Data on Intrinsic Conductances." *Journal of Neurophysiology*, vol. 66, no. 2, 1991, pp. 635–650., doi:10.1152/jn.1991.66.2.635.

[50] S. Intep and D. J. Higham, Zero, one and two-switch models of gene regulation, *Discrete and Continuous Dynamical Systems-Series B*, 14 (2010), 495-513.

[51] G. De Vries and A. Sherman, Channel sharing in pancreatic β-cell revisited: enhancement of emergent bursting by noise, *J. Theor. Biol.*, 207 (2000), 513-530.

[52] M. I. Freidlin, Quasi-deterministic approximation, metastability and stochastic resonance, *Phys. D*, 137 (2000), 333-352.

[53] L. Gammaitoni, P. Hanggi, P. Jung and F. Marchesoni, Stochastic resonance, *Rev. Mod. Phys.*, 70 (1998), 223-287.

[54] T. Wellens, V. Shatokhin and A. Buchleitner, Stochastic resonance, Rep. Prog. Phys., 67 (2004), 45-105.

[55] I. Atwater, L. Rosario and E. Rojas, Properties of the Ca-activated K+ channel in pancreatic beta-cells, Cell Calcium, 4 (1983), 451-461.

[56] T. R. Chay and H. S. Kang, Role of single-channel stochastic noise on bursting clusters of pancreatic_-cells, Biophys. J., 54 (1988), 427-435.

[57] A. Sherman, J. Rinzel and J. Keizer, Emergence of organized bursting in clusters of pancreatic beta-cells by channel sharing, Biophys. J., 54 (1988), 411-425.

[58] M. Pedersen and M. Serensen, The effect of noise on β-cell burst period, SIAM J. Appl. Math., 67 (2007), 530-542.

[59] J. Su, J. Rubin and D. Terman, Effects of noise on elliptic bursters, Nonlinearity, 17 (2004),133-157.

[60] Kuske, R.and Baer, S. M. Asymptotic analysis of noise sensitivity in a neuronal burster *Bulletin of Mathematical Biology* (2002)

[61] Jianzhong Su, Humberto Perez-Gonzalez, Ming He. Regular bursting emerging from coupled chaotic neurons. Conference Publications, 2007, 2007 (Special): 946-955.doi: 10.3934/proc.2007.2007.946

BIOGRAPHICAL STATEMENT

Ariel Leslie was born and raised in Dallas, TX as Ariel Bowman. She graduated from Plano East Senior High School June 2010. Ariel then went on to earn her Bachelors degree in Mathematics in 2014 from Texas Southern University in Houston, TX. Due to her love of health and passion for knowledge of disease, she also obtained her minor in Health Studies. Fall of 2014, Ariel Leslie began her graduate studies at University of Texas at Arlington in the Department of Mathematics. At UTA, she and another graduate student co-founded a business by the name of ESTe^2M Builders.